CRANFIELD UNIVERSITY

Fabian Duarte Martinez

Understanding nanoscale material behaviour for improved precision machining of shape memory alloys: Testbed study on elliptical vibration assisted cutting of CuZr SMA

School of Aerospace, Transport and Manufacturing

MRes in Ultra Precision Engineering

Master of Research

Academic Year: 2016 - 2017

Supervisor: Dr Saurav Goel

Associate Supervisor: Dr Kostas Georgarakis

01/2018

CRANFIELD UNIVERSITY

School of Aerospace, Transport and Manufacturing
MRes in Ultra Precision Engineering

Master of Research

Academic Year 2016 - 2017

Fabian Duarte Martinez

Understanding nanoscale material behaviour for improved precision machining of shape memory alloys: Testbed study on elliptical vibration assisted cutting of CuZr SMA

Supervisor: Dr Saurav Goel
Second supervisor: Dr Kostas Georgarakis
January 2018

This report is submitted in partial fulfilment of the requirements for the degree of MRes in Ultra Precision Engineering

ABSTRACT

The field of ultra-precision machining has gained significant importance in the manufacture of components for the electronic, optical and medical industry. Two crucial factors that play a key role in the machinability of materials are the machining parameters and the material's physical properties. Certain materials such as hardened steel or nickel-based superalloys are difficult-to-machine but innovations in the field of precision machining have developed a technique known as elliptical vibration assisted machining, which enables to improve the machinability of these materials. CuZr high-temperature shape memory alloy is categorized as a difficult-to-cut material and although EVAM has been applied to a wide range of metals it hasn't yet been studied in CuZr HTSMA. In this context, the purpose of this thesis is twofold: On the one hand, to characterise the mechanical properties of CuZr SMA using Molecular Dynamics and, on the other hand, to explore the nanoscale mechanism of material removal of CuZr shape memory alloy (SMA) during elliptical vibration assisted machining (EVAM). The conclusions of this thesis can be summarized as follows.

To characterise the mechanical properties of $Cu_{50}Zr_{50}$, Cu_2Zr and Cu_5Zr, a tensile and shear test were carried out using MD. Tensile test was done with crystal orientation and direction of tensile pulling as <010>. The results showed that $Cu_{50}Zr_{50}$ and Cu_2Zr exhibited a phase transformation (pseudoelasticity) during loading. However, Cu_5Zr showed dislocation nucleation as the main plastic deformation mechanism followed by fracture.

Shear tests were done in the same phases with crystal orientation and direction of shear pulling as <100>. Interestingly, the shear test results showed no phase transformation for $Cu_{50}Zr_{50}$ and Cu_2Zr but the Cu_5Zr composition did show phase transformation during loading. It is important to highlight that all three phases of CuZr binary alloy that we have tested showed a different plastic response during the tensile test and the shear test.

As far as machining is concerned, we observed indications that EVAM shows improved machinability compared with conventional machining. Although cutting forces were lower in EVAM, the stresses on the workpiece were slightly higher

and both techniques showed the same mechanism of plasticity during machining. Neither dislocation nucleation or martensitic transformation was exhibited in either of the two machining techniques and instead, amorphisation was observed as the main plastic deformation mechanism in both cases. Interestingly, amorphisation has been previously observed by Saitoh and Kubota (2010) during loading NiTi SMA [1]; however, it didn't show up in every crystal orientation confirming that NiTi shows significant changes in response to loading in different lattice directions.

One of the main outcomes from this thesis is that CuZr SMA exhibits different modes of plastic deformation; namely amorphisation, dislocation nucleation and martensitic transformation during loading. The governing mechanism that arises during loading highly depends in the lattice direction in which the load is being applied. These findings can potentially enable reliable predictions and provide guidelines of the microstructural design of CuZr SMA systems.

ACKNOWLEDGEMENTS

Firstly, I would like to give my sincere thanks to EPSRC for funding my MRes program and the Centre for Doctoral Training (CDT) for providing me with the required skill sets towards my engineering career.

A special thanks to my supervisor, who has guided me through this thesis and gave great support towards my learning experience. He helped in all aspects throughout this project, from my learning in simulation techniques to materials science and continuously shared his research experience, which was of excellent value. Also, a great thanks to Dr Konstantinos Georgarakis, who shared his expertise in metallurgy and made himself available to help me whenever I needed.

I would like to thank Michael Knaggs from HPC team and IT staff members at Cranfield University for providing me with great assistance with Delta HPC service which was highly useful throughout my thesis.

Finally, I would like to thank my family who continue to provide their great support in my academic career.

TABLE OF CONTENTS

LIST OF TABLES

LIST OF FIGURES

LIST OF SYMBOLS

A_s: Austenite start temperature

A_f: Austenite finish temperature

M_s: Martensite start temperature

M_f: Martensite finish temperature

LIST OF ABBREVIATIONS

SMA: Shape memory alloy

SME: Shape memory affect

HTSMA: High-temperature shape memory alloy

MD: Molecular Dynamics

NVE: Constant number of particles, volume and energy in a system

NVT: Constant number of particles volume and temperature in a system

NPT: Constant number of particles, pressure and temperature in a system

NiTi: Nickel-Titanium

CuZr: Copper-Zirconium

VAM: Vibration assisted machining

EVAM: Elliptical vibration assisted machining

EAM: Embedded atom method

MEAM: Modified embedded atom method

2NN MEAM: Second nearest neighbours modified embedded atom method

BCC: Body centred cubic

FCC: Face centred cubic

PTM: Polyhedral template matching

CNA: Common neighbour analysis

1 INTRODUCTION

1.1 Scope of work

Metallurgy is a domain of materials engineering concerned with the behaviour of metallic elements. Advances in this field have enabled remarkable progress in structural engineering in the last 50 years. Among the vast type of metallic systems, one of the main materials leading this field are shape memory alloys (SMA).

Shape memory alloys are categorized as smart materials due to their ability of returning to a predefined shape when heated or stressed. This behaviour is known as shape memory behaviour and is caused by a diffusionless phase transformation between a parent austenite and a martensite phase. The shape memory effect in these metals enables them to be used as actuators to produce movement more efficiently than conventional technologies. For instance, shape memory alloys have a higher power to weight ratio, are noiseless and don't require parts such as dampers or spring-deployed structures, making their design very simple in comparison with conventional actuator technologies. For this reason, they are replacing products such as electric motors, solenoids and piezo electric actuators.

One of the emerging applications of these material are in actuators operating in hot temperature environments. High-temperature shape memory alloys, such as CuZr binary alloy, exhibit a series of interesting mechanical properties that are worth considering when operating at elevated temperatures and understanding its deformation behaviour at atomic scales can provide key information in product design stages. For this reason, the first objective of this work is to characterise the mechanical properties of CuZr SMA during tension and shear testing using Molecular Dynamics.

Also, in the last 20 years there has been an increase in the use of shape memory alloys particularly in the automobile and medical industry; hence different manufacturing techniques have been considered to produce them in mass scales. The ultimate goal in their manufacturing process is to produce a precise final shape, control their transformation temperature, and to preserve its shape

memory effect [2]. Conventional machining techniques have often been regarded as a low-cost technique (in comparison with non-conventional machining processes), with easy set-up and easily adoptable in industry; therefore, a very attractive manufacturing technique. However, material properties such as strain hardening, fatigue hardening, high toughness, pseudoelasticity and shape memory effect make shape memory alloys difficult to be machined. The reason why these material properties involve challenges during machining will be further explored in a later section.

Although it is challenging to machine shape memory alloys by conventional means, a technique known as intermittent cutting has proven useful to machine difficult-to-cut materials such as hardened steel, but it hasn't been extensively applied to shape memory alloys. Intermittent cutting consists in applying oscillatory motion to the tool so that it vibrates and hence is not in continuous contact with the workpiece. To achieve this, the tool can either move with linear vibration motion (1D VAM) or with an elliptical vibration assisted motion (EVAM). The literature suggests that both these techniques show considerable improvements in machinability compared with conventional machining.

There has been very limited work evaluating the machinability performance of shape memory alloys using intermittent cutting and no work so far on CuZr binary alloy, which is a suitable alloy for high-temperature actuator applications with a low cost of raw material and very good casting fluidity at high temperature [3]. For this reason, the aim of this thesis is to compare the machinability performance of conventional machining and EVAM of CuZr shape memory alloy from an atomistic perspective.

To evaluate the machinability of a material one of the key features that should be studied is how the material plastically deforms during machining. A thorough study of the plastic behaviour of materials can generally provide a good indication of the cutting forces, temperature gradients and interactions between the tool and workpiece, which are directly linked with the surface finish and dimensional accuracy of the machined workpiece.

Although significant work has been undertaken to study the advantages of intermittent cutting over conventional machining, there is still a lack of

understanding of the fundamental plasticity mechanisms in the workpiece that lead to this improvement in machinability. For that reason, one of the main questions that I want to address is what atomic scale mechanisms take place during elliptical vibration assisted machining that lead to this improvement, if any, in machinability.

To compare these two techniques, molecular dynamics will again be used to study the atomic trajectories and fundamental mechanisms of plasticity during machining. This will enable us to further understand the phenomena that leads to any possible differences in machinability when using elliptical vibration assisted machining as opposed to conventional machining.

1.2 Aims and objectives

The aim of this thesis is twofold. Firstly, we aim to characterise the mechanical properties of CuZr SMA, and secondly, to understand the nanoscale microstructural response of CuZr SMA during EVAM and conventional machining.

The first objective is to characterise the mechanical properties of CuZr binary alloy by running a tensile and shear test simulation using molecular dynamics in three phases of CuZr binary alloy, namely $Cu_{50}Zr_{50}$, $CuZr_2$ and Cu_5Zr. Some of the key deliverables that are considered are the maximum recoverable strain, critical stress of phase transformation and the effect of temperature in the stress-strain relationship of CuZr binary alloy. These deliverables will aid in developing a fundamental understanding of the pseudoelastic behaviour of CuZr binary alloy.

Ultimately, the final objective is to run a molecular dynamic simulation of EVAM and conventional machining of $Cu_{50}Zr_{50}$ SMA and study the nanoscale material removal mechanism using tools such as Dislocation Extraction Algorithm (DXA) and Common Neighbour Analysis (CNA).

1.3 Research questions

1. What are the differences in mechanical properties of distinct phases of CuZr binary alloy and do these phases exhibit shape memory effect?

2. What is the mechanism governing plasticity in distinct phase of CuZr during tensile and shear test?
3. How does the plasticity augment and compare during EVAM of CuZr shape memory alloy to conventional machining?

1.4 Structure of the report

The second chapter will provide an overview of the field of shape, memory alloys, fundamentals of intermittent cutting and simulation tools to study plasticity in machining. The first section of chapter two will describe a historical background of shape memory alloys, highlight recent work done in this field and describe some of the applications where SMA are used.

The second section of chapter two will define the fundamental concepts in machining and provide an overview and the advantages of elliptical vibration machining over conventional machining. Within this section I will highlight the main difficult-to-cut materials that have been evaluated using EVAM and define the effect of reverse friction, which is one of the key features that leads to an improved machinability.

The last section of chapter two will define what molecular dynamics is, its analytical framework and how it can play a role in further understanding the atomic-scale mechanisms of plasticity. I will define the concept and significance of identifying an optimum interatomic potential function and describe the 2NN MEAM interatomic potential function that has been used to model CuZr binary alloy in this simulation.

Chapters four, five and six will evaluate and discuss the results obtained of mechanical characterization of CuZr crystalline alloy as well as the results obtained in EVAM and conventional machining.

2 LITERATURE REVIEW

2.1 Historical background of shape memory alloys

Shape memory alloys are metallic systems that, once deformed, can return to their original shape by applying heat or stress. These alloys were discovered in 1932 by Arne Olande Otsuka and Wayman when they observed the pseudoelastic effect in AuCd alloy, which is an elastic response of a material caused by a phase transformation when stressed. The first industrial application of SMA was in 1967, where it was used as a coupling sleeve Raychem for a F-14 aircraft. Since then, shape memory alloys have been used in fields such as textile, aeronautics, automotive and biomedical industry. Within these fields, shape memory alloys have generally been used as actuators in environments that require a change in shape and stiffness due to a change in temperature, stress or electromagnetic field.

Shape memory alloys can “remember their shape” when heated or stressed due to a diffusionless[1] phase transformation between austenite (parent phase) and martensite. The austenite to martensite phase transformation in SMA is known as a displacive phase transformation, which involves the coordinated motion of several atoms relative to its neighbours. Although this coordinated movement is very small, its effect at the macro-scale is significant.

The phase transformation can be temperature-induced, stress-induced or a combination of both. Figure 1 shows a temperature induced phase transformation in SMA. When stress free, the temperature in which martensite starts to form upon cooling is known as the M_s and the temperature in which the transition to martensite is complete is M_f. Similarly, the temperature in which austenite starts to form upon heating is known as A_s and the temperature in which austenite has completed forming is A_f. In few words, below the temperature M_f, the twinned martensite phase is stable and for temperatures higher than A_f, the austenite structure is the most stable phase [4].

[1] Diffusionless phase transformation in SMA is one in which a of atoms move cooperatively relative to their neighbours by a mechanism known as twinning that results in a change in crystal structure.

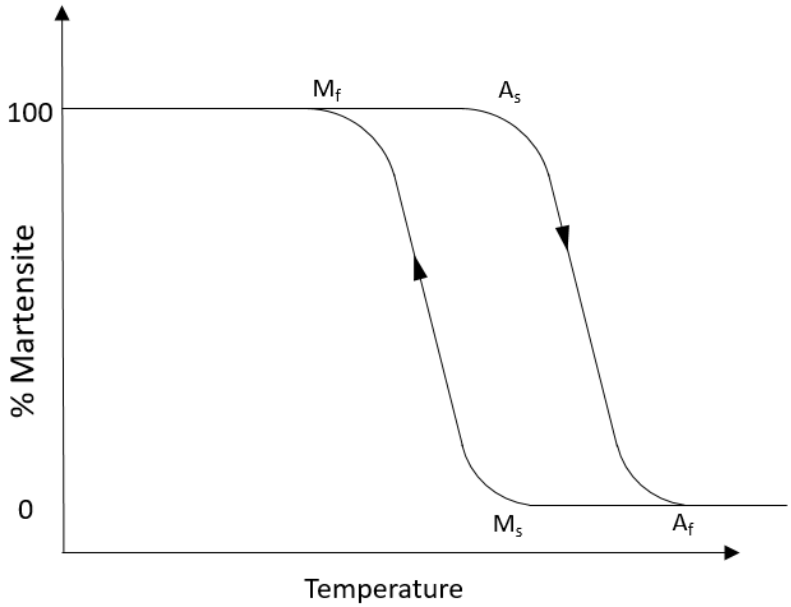

Figure 1 - Temperature induced phase transformation

For temperature induced transformations free of stresses, if we cooled a single crystal parent austenite face below M_s, a single crystal of martensite with various twin related variants and with different crystallographic orientations is formed [5] [6]. These twins are separated by mobile twin boundaries that have low energy [7]; therefore, if at this stage we applied a stress in the martensite phase, deformation takes place by reorientation of the variants through the movement of the twin boundaries. In simple terms, applying a stress enables us to selectively grow one specific variant (the variant most favourably oriented to the direction of loading) of martensite and this process is known as detwinning, which enables to obtain large inelastic strain. After removing the stress and increasing the temperature to A_f, the boundaries move back to restore the original shape, hence recovering the inelastic strain of the material. This mechanism just described is illustrated in Figure 2 and is key for the shape memory effect to take place.

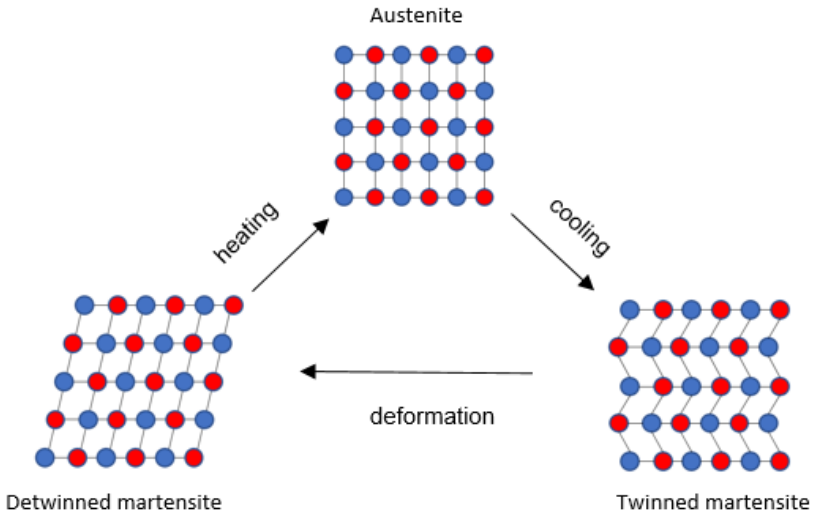

Figure 2 - Shape memory effect in shape memory alloys

In the case where the phase transformation is stress induced and no temperature change takes place, an applied stress in the austenitic phase will directly transform austenite into detwinned martensite.

The stress induced phase transformation leads to another remarkable advantage of shape memory alloys, which is the high elastic strains they can withstand. The stress-induced phase transformation leads to the behaviour known as the pseudoelastic effect. Pseudoelasticity also takes place due to a diffusionless phase transformation. When a critical stress is applied in a shape memory alloy in its austenite phase it will transform into martensite. As shown in Figure 3, the critical stress in which the austenite to martensite phase transformation occurs is labelled as σ^{Ms} and the stress in which martensite has completely formed is denoted as σ^{Mf}. If we release the stress at this point, the martensite phase will revert to its austenite phase enabling the material to recover its initial shape.

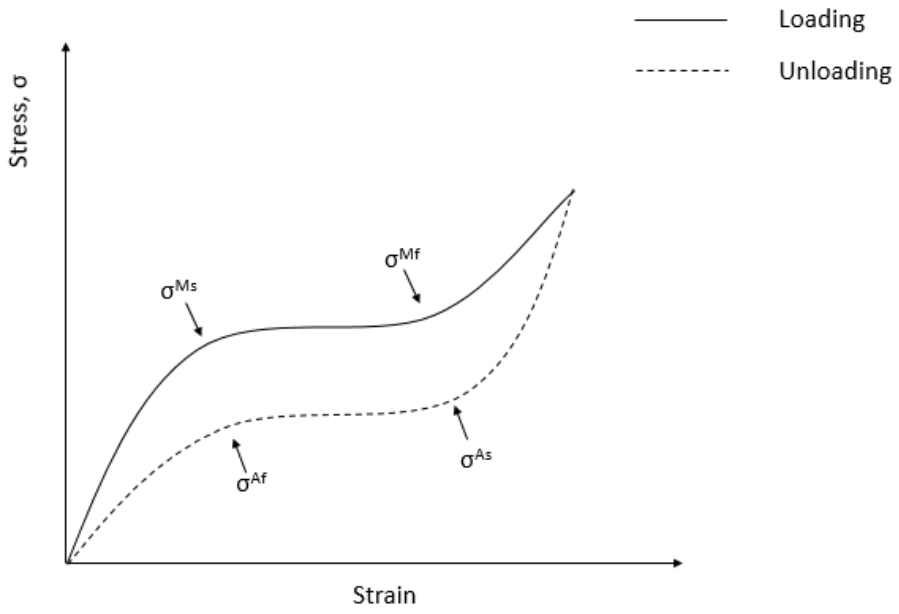

Figure 3 - Pseudoelastic effect in shape memory alloys

The alloy compositions that have attracted considerable attention to fabricate shape memory alloy components are Ni-based and Copper-based shape memory alloys. For instance, NiTi binary alloy has shown the most optimum material properties for shape memory alloys due to their higher strength, fatigue resistance, high ductility, biocompatibility and wear resistance in comparison with most other alloy systems but NiTi alloy is considerably more expensive [8]. As an alternative lower-cost option, copper-based shape memory alloys have also attracted interested; however, the main issue with Cu-based SMA is their low ductility, which poses considerable challenges during manufacturing and in using them in structural applications.

Let us further examine these two systems. NiTi have very high recoverable strains (strains up to 7%), higher strength, more phase stability and other physical properties, which makes them the primary choice for structural applications. Table 1 highlights some of the differences in mechanical properties between NiTi base alloy and a well-known Cu base shape memory alloy alloys.

Table 1 - Comparison in mechanical properties between NiTi and CuZnAl [9]

	NiTi	**CuZnAl**
Recovery strain	8%	4%
Recovery stress	500 MPa	200 MPa
Corrosion resistance	Good	Problematic

By changing the composition of NiTi we can greatly affect the temperature in which the phase transformation takes place (roughly between the range of -200 to 200ºC) [10]. This means that a slight change of composition has a significant effect in phase transformation temperatures, therefore the processing of NiTi must be precisely controlled. Also, to avoid the formation of oxides, nitrides and carbides, NiTi is normally processed using vacuum melting process and this makes the production of NiTi samples considerably expensive [10]. One of the main advantages of NiTi SMA is its high corrosion resistance due to the passive TiO_2 film that forms in its surface [10].

The other types of SMA metallic systems that are of commercial interest are copper based shape memory alloys. These alloys have a maximum recoverable strain of approximately 5%, which is very high compared to most SMA compositions but not as high as NiTi alloy [11]. On one hand, a major disadvantage of copper-based shape memory alloys is their large grain sizes, which makes them brittle. For this reason, grain control additives are normally introduced. On the other hand, the main advantages of copper-based shape memory alloys are the low cost of raw materials and the fact that they can be processed using low cost techniques such as induction melting.

One emerging field is the use of high-temperature shape memory alloys (HTSMA), which require stable phase transformation temperatures above 390K [12]. HTSMA are of increasing interest in fields such as aerospace, automotive and energy, which require actuators to be used at these high-temperatures. One of the early applications of HTSMA was in thermal protection devices, where these alloys are designed to output signals when sensing overheating [13].

Potential applications of HTSMA include actuating systems in aerospace propulsion technologies and automotive applications around the engine; however, applications in aerospace require transformation temperatures (TT) in the range of 200-1000 ºC and in automotive applications the required transformation temperature is between 100-300 ºC [14].

Research efforts are focusing in testing different compositions to increase the attainable TT and retain properties such as the shape memory effect. For instance, the transformation temperature for the commercially available NiTi alloy is below 100 but adding elements such as Au, Pd, Pt, Hf and Hr it is possible to increase the transformation temperature (TT) [15]. Although potential research efforts are being done to increase the TT of NiTi base alloys, they still involve a high-cost of raw material. As an alternative, Cu based alloys are offering high transformation temperatures at a low cost of raw materials. However, they still come at the expensive of low ductility.

The alloy composition that will be considered in this thesis is CuZr binary alloy due to its high-temperature phase transformation, its low cost of raw material and its high casting fluidity at high-temperature.

A major application of SMA and particularly CuZr SMA has been to use them as a reinforcement in metallic glasses[2]. The $Cu_{50}Zr_{50}$ composition can be synthesized into a metallic glass and it is a very important alloy due to its significantly low critical cooling rate[3]. The way in which metallic glasses plastically deform is by the nucleation and propagation of shear bands[4]. Although this mechanism of plastic deformation has been studied for several years, the formation and propagation of shear bands is still poorly understood and is currently a subject of intense research. An approach to overcome the poor ductility of CuZr metallic glass is to introduce CuZr SMA crystal phases to act as

[2] Metallic glasses are metals with an amorphous structure as opposed to a crystalline structure, which show remarkable mechanical, electrical and magnetic properties but their limitation is that they suffer from low ductility.

[3] Critical cooling rate is the minimum rate of continuous cooling that must be applied to a metal to supress undesired transformations such as crystallization.

[4] A shear band is a narrow zone of high strain due to shear experienced by certain materials when they are severely deformed.

strong barriers for the propagation of shear bands and thus enhance the plasticity of the metallic glass [16].

There are a wide range of processing techniques to manufacture shape memory alloy components. Unconventional machining techniques have offered remarkable advantages to process these materials. Some unconventional techniques include electrical discharge machining, which can be used to machine materials of any hardness, brittle materials and have very high dimensional precision [17]. Likewise, laser machining enables very hard and brittles materials to be accurately machined with no tool wear and a very narrow heat affected zone. Waterjet cutting offers very high machining accuracies and does not generate heat, which is significantly important as heat can play a role in changing the properties of the shape memory alloys during the machining process.

Although unconventional machining offers some great advantages over conventional machining techniques, they generally have a higher cost, a more complex set-up and requires highly skilled labour compared with conventional machining techniques. For that reason, conventional machining techniques will be the preferred option only if they offer the capability of machining a component to the desired specifications. Having said this, innovations in the field of conventional machining enables to process difficult-to-cut materials like shape memory alloys using a technique known as intermittent cutting.

If we consider conventional machining techniques to process shape memory alloys, some of the material properties that make it difficult to machine is the pseudoelastic effect, strain hardening and the toughness of the material.

The pseudoelastic effect is caused by an austenite to martensite phase transformation when high enough resolved shear stress is applied to cause this change in microstructure. The problem in machining martensite is that it has a higher hardness than the austenite phase, which increases the tool wear and heat at the cutting tip. In addition, an increase in hardness leads to an increase in the force needed to cut the chip, which leads to deflection problems during machining and chatter that can lead to considerable damage in the tool and workpiece [18].

Strain hardening refers to the strengthening of a metallic system caused by plastic deformation. This is problematic during machining because as the cutting tool removes material it strengthens the surface of the workpiece causing damage to the tool in later passes.

Toughness is also a critical material property in the field of machining and it refers to the amount of energy that a material can absorb to plastically deform without fracturing. In the field of machining its important because the higher the toughness the higher the forces need to be to break down the material. For that reason, high toughness is not desired as it reduces the machinability of a material [19].

Previous research confirms that intermittent cutting techniques have a major effect in decreasing cutting forces in comparison with conventional machining. However, the mechanisms that lead to this decrease in cutting forces is not well understood. Using experimental techniques to understand the microstructural changes of materials during machining can provide great insight but unfortunately, they are limiting to understand the fundamental mechanisms of plasticity, which is vital to compare two different machining techniques. For this reason, atomistic simulation has proven to play a pivotal role in unravelling atomic-scale behaviour which is challenging to study experimentally.

Understanding the improvement in machinability of EVAM compared with conventional machining by experimental means is difficult. Chip formation, cutting forces and temperature gradient provide good insight into the machinability of materials and they highly dependent on the plasticity mechanism of a material. For that reason, studying the mechanisms of plasticity at atomic scales can provide a good indication for any differences between EVAM and conventional machining. For instance, a decrease in the cutting forces in EVAM may be due to an increase in dislocation density or perhaps a change in plastic deformation mechanism such as from phase transformation to twinning. However, to understand the mechanisms of plasticity it is necessary to analyse them at atomic scales. Studying these mechanisms of plasticity experimentally can be very challenging and costly, therefore simulation techniques can play a vital role in understanding these mechanisms.

2.1.1 Applications of shape memory alloys

Within the field of biomedical sciences and odontology, shape memory alloys are used for mending bones, as dental wires and reinforcing arteries.

Shape memory alloys can be used as micro-actuators. The large recoverable strain in SMA enables them to apply recovery forces in a specific direction as the and this force can be used to do work. Shape memory alloys can be defined as thermal actuators as they enable us to convert thermal energy directly into mechanical energy. A few advantages of the use of SMA as actuators is their high power to weight ratio and their silent working conditions as there is no friction or parts vibrating [20]. One of the fields of current research is using the actuation functionality of SMA in soft-grip applications. Figure 4 shows the implementation of SMA in prosthetic fingers, where the use of SMA has reduced significantly the number of motors and reduced the weight of the whole mechanism [21].

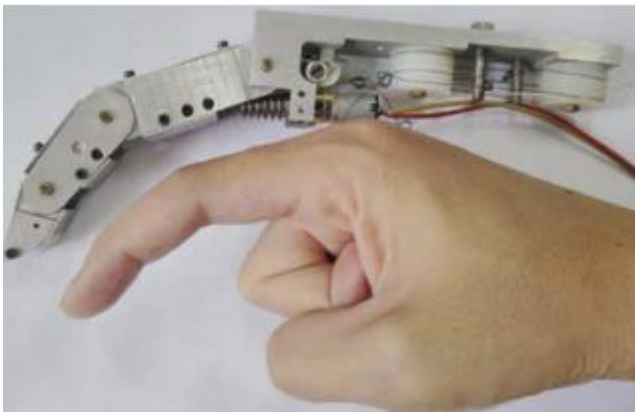

Figure 4 - Tendon-driven underactuated prosthetic fingers [21].

Shape memory alloys can be used to join bone fragments. During the bone healing process, there is a change in stiffness of the bone and according to Wolf's law, an implant that is able to change its stiffness in the same degree as the bone will help significantly in bearing loads during the recovery process and hence facilitate bone recovery [22]. Shape memory alloys are now used as implants in this specific field as they can change its stiffness at a specific time. Figure 5 shows a NiTi SMA implant that can effectively alter its bending stiffness and hence used to join bone fragments.

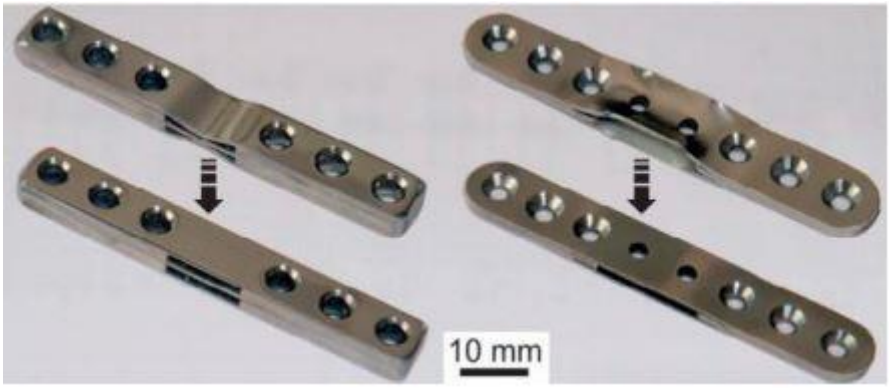

Figure 5 - NiTi SMA implant sample [23]

Shape memory alloys are used as spinal rods to keep the spinal force loaded after an operation, helping significantly with scoliosis correction. Figure 6 shows the change in shape of a spinal rod after applying heat.

Figure 6 - Spinal rod. The first image shows the straightened rod with anchorage system and the second image shows the original curve of the rod after applying heat [24].

Shape memory alloys are used as dental arch wires in dental applications. To enable dental corrections, the force from the braces must lie in a certain range. If the force is too high, it may lead to the absorption of the bone and if the force is too low then dental correction may not take place. The pseudoelastic effect of shape memory alloys is useful as it enables the alloy to return to their original shape during unloading by providing light and continuous forces, which is in the optimum range for dental correction.

A major application of shape memory alloys is in tracking rotor blades. During the manufacturing processes the aerodynamic contour, mass and centre of gravity of rotor blades may vary slightly from blade to blade and this difference can be quite significant when blades are made of plastic reinforced composites. These differences are disadvantageous as it causes unwanted vibrations which lead to lower fatigue life of the blade and reduces the ride comfort [25]. The conventional

method to track rotor blades is ground based and normally requires complex manual adjustments. The use of shape memory alloys in rotor blades enables deflecting and tracking the blades in-flight, which replaces manual tracking methods, reduces maintenance cost, operation errors and other costs [25].

Shape memory alloys are also used in aircraft wings to change the wing's shape or geometry during flight, which is a key feature that helps to optimise the wing's aerodynamic performance and hence reduce fuel consumption. Figure 7 shows a cellular flexible core between shape memory alloy sheets. The main idea is to apply heat to either of the SMA sheets, which will cause contraction and hence generate a curvature in the actuator.

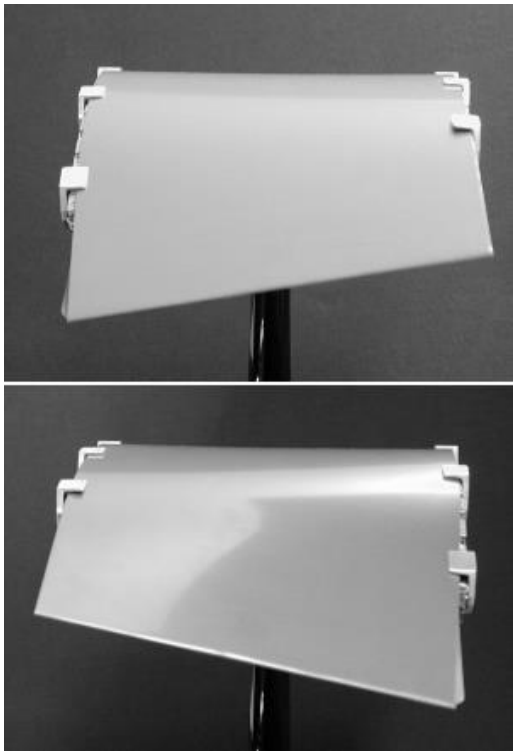

Figure 7 - Cellular flexible core between SMA sheets for aircraft morphing [26]

2.2 Fundamentals of intermittent cutting

Metal cutting consists in removing excess material from a metal using a cutting tool to convert the remaining material into a desired shaped component. The forces acting on the tool and workpiece during the chip formation plays a key role in the final quality of machined surface, tool wear and geometrical accuracy of the machined component. The key factors that determines the chip formation forces is the material properties of the workpiece and tool geometry. However,

there are other factors such as cutting speed and feed rate that influence the strength of the material in the deformation zone by causing changes in temperature or strain hardening [27]. For instance, during turning the strain rates experienced by a material is of the order of 10^3 s^{-1} or higher. Some materials may be very sensitive to strain hardening effects therefore careful selection of machining parameters that affect the strain rate during machining is of critical importance.

There is a wide range of difficult-to-cut materials such as hardened steel, tungsten carbide, silicon, nickel-based superalloys and ferrous alloys, which are of huge importance in many sectors and their processability is often a challenge. Generally, these materials have been processed using non-conventional techniques but some of these techniques either involve an excessive cost, slow processing times or other difficulties. For this reason, machining techniques can be considerably useful as they offer a lower cost, faster processing times and easily adoptable in industry. However, some of the key issues in machining these materials are their high hardness, brittleness, low thermal conductivity and work hardening properties, which can ultimately lead to rapid tool wear, subsurface damage and poor surface roughness.

Innovations in the field of machining have enabled the processing of these materials using a technique known as intermittent cutting. Intermittent cutting consists in setting an oscillatory motion on the tool during the machining process so that the tool is not in continuous contact with the workpiece. This technique has proven to reduce cutting forces, increase the shear angle, wear rate, reduce burr formation and has also enabled to perform ductile regime machining using higher depths of cut compared with conventional machining techniques.

Vibration assisted machining can either be one-dimensional (1D VAM) or two-dimensional (2D VAM) and current research is focused in developing 3D VAM. In 1D VAM, the tool vibrates in a plane parallel to the surface of the workpiece. In 2D VAM, the tool vibrates with an elliptical motion, therefore this technique is also known as elliptical vibration assisted machining (EVAM). These two types of motion yield different machining performances and have been compared in several reports.

In EVAM, the major axis of the ellipse is in the same direction as the cutting force and the minor axis of the ellipse is in the same direction as the thrust force [28]. Although VAM already shows remarkable improvements in machinability performance in comparison with conventional cutting, EVAM makes further improvements in several aspects. 1D and 2D VAM can either be resonant based and non-resonant based. On one hand, the resonant system operates at discrete frequencies, normally higher than 20 kHz and amplitudes less than 6µm. On the other hand, the non-resonant system operates at a frequency range between 1-40 kHz and amplitudes ten times higher than the resonant system [28].

2.2.1 1D Vibration-Assisted machining

Vibration Assisted Machining (VAM) is a technique that adds an amplitude and frequency to the displacement of the tool. This linear harmonic motion causes the tool to periodically loose contact with the workpiece for approximately 75% of the processing time, which in turn, reduces the chip thickness and the cutting forces substantially. Low cutting forces lead to a reduction in stress, strain and temperature in the machined zone. As a consequence, there is a reduction in burr formation, an improvement in surface finish, an extended lifetime of the tool and an improved form accuracy in comparison with conventional cutting techniques. [29]. Figure 8 and Figure 9 shows an illustration of the tool movement and variation in cutting force in 1D VAM compared with conventional machining.

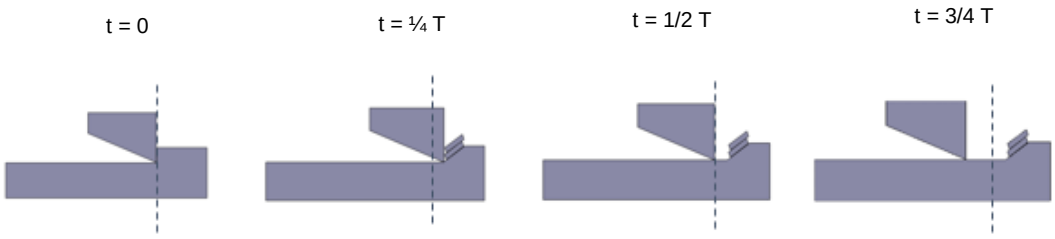

Figure 8 - 1D VAM

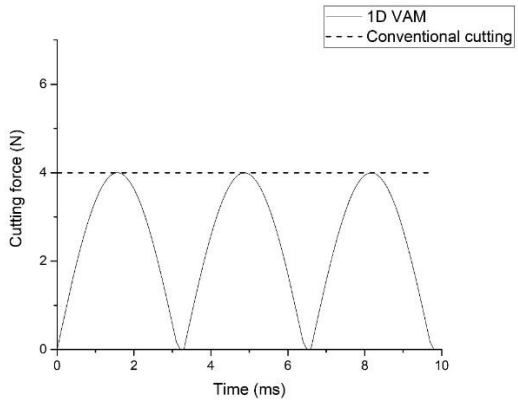

Figure 9 - Variation in cutting force in 1D VAM and conventional machining

As can be observed in Figure 9, the cutting force in VAM is oscillating while the peak cutting force in VAM and conventional machining are the same. This oscillation causes the average cutting force in VAM to decrease significantly.

One of the main advantages of the decrease in cutting force is that it enables to machine brittle materials using ductile regime machining. Several reports highlight that this technique enables ductile mode machining (DMM) at higher depths of cut compared with conventional diamond cutting techniques [29]. The interesting fact about VAM is that small cutting forces enable to reduce the depth below the machined surface in which micro-fractures generate and propagate. In few words, it enables to operate at higher depths of cut without fracturing the sample. Increasing the critical depth of cut can bring certain advantages as it does not require expensive ultra-precision tools, highly skilled labour and enables an increase in the material removal rate (MRR).

VAM enables lower temperatures in the cutting zone in comparison with conventional cutting (CC). During the cutting process, the tool loses contact with the workpiece in a periodic fashion, therefore the tool is separated from the primary and secondary deformation zones for a certain amount of time in each cutting cycle, causing a substantial temperature decrease. This advantage plays a considerable role in reducing tool wear and enables the cutting of materials with low thermal conductivity and high heat capacity such as titanium alloys [30].

There are two ways in which VAM can be performed in a turning process. The vibrations can be performed in the tangential direction or in the feed direction. When vibrations take place in the tangential direction, there is a separation

between the tool and the chip. When vibrations take place in the feed direction, the separation occurs between the tool and the whole workpiece [31]. Manikandakumar et al. (2014) report that vibrations in the tangential direction decrease cutting forces whereas the vibrations in the feed direction improves the finished surface [31].

An important term in VAM is tool workpiece contact ratio (TWCR). TWCR refers to the ratio of the time that the tool is in contact with the workpiece and the time it takes the tool to complete one vibration cycle. Several reports suggest that decreasing TWCR decreases the cutting forces significantly. It has also been reported that increasing the amplitude and frequency leads to a lower TWCR and hence a reduction in cutting forces. Studying the variations of amplitude and frequency has been one of the frontiers in exploiting the full advantages of VAM. The TWCR is expressed using the following equation.

$$TWCR = \frac{t_c}{t}$$

Where t_c is the contact time and t is the time it takes the tool to complete one cycle. Several papers report that increasing the frequency and amplitude leads to a lower TWCR, therefore an improved machinability performance. Sharma et al (2013) tested different amplitudes and frequencies in ultrasonic assisted turning (UAT) to reach optimum machining conditions. For instance, by maintaining the frequency constant and increasing the amplitude up until a critical value would decrease the cutting forces. Beyond this critical amplitude, no decrease in cutting force was observed [32]. An additional consideration is that the maximum vibration velocity of the tool should be equal or higher to the cutting speed. This is expressed in the following equation [32].

$$v_{max} \geq v_c \qquad (1)$$

$$\omega A \geq v_c \quad (2)$$

Where v_{max} is the maximum vibration velocity of the tool, A is the amplitude, ω is the angular velocity of the tool and v_c is the cutting speed.

The critical cutting speed sets a limit in UAT and UEAT; therefore, these techniques are categorized as low speed machining techniques and can't be applied to high speed machining applications [30].

Overall, VAM and EVAM have had major impact in the field of machining. Table 2 shows some of the applications where VAM and EVAM had a considerable influence in the last seven years.

Table 2 - Applications in VAM and EVAM in the last 7 years

Authors of the article	**Material**	**Parameters (feed rate (F_r), cutting speed (v), depth of cut (d)).**	**Oscillation parameters (frequency (f), amplitude (a))**	**Cutting force comparison with conventional turning**	**Additional conclusions**
Muhammad et al. (2014) [33]	Ti6Al2Sn4Zr6Mo (α+β Ti alloy)	f_r = 0.1 mm/rev; v = 10-60 m/min; d = 0.2mm	f = 20kHz; a = 10 µm	74% reduction	50% in surface roughness.
Muhammad et al. (2014) [34]	Ti-15333 (β alloy)	f_r = 100 µm/rev; v = 10m/min; d =100-500 µm	F = 20 kHz a = 8 µm	80-85% reduction	50% reduction in surface roughness; Heat is applied during ultrasonic assisted machining
Patil et al. (2014) [35]	Ti6Al4V	f_r = 0.1mm/rev; v = 10-300m/min d = 0.1mm	f = 20 kHz a = 20µm	40-45% reduction	Reduction of 40% In surface roughness
Mourotto et al. (2013) [36]	Ti 15-3-3-3 (β Ti-alloy)	F_r = 0.1mm/rev; v = 10-70m/min; d = 50-500 µm	f = 17.9 kHz a = 10 µm	71%-88% reduction	Reduction of 49% in surface roughness
Noth et al. (2007) [37]	Low alloy steel (DF2)	F_r = 0.1mm/rev; v = 50m/min; d = 0.2mm	F = 19 kHz; a = 15 µm	50% reduction	Tool wear 20% less than in CT.

2.2.2 Mechanics of cutting force reduction and of tool wear reduction

The reduction in cutting forces arises from changes in the workpiece and tool's microstructure when exposed to ultrasonic vibration fields. Changes in friction during cutting have also been reported as causes leading to a reduction in cutting forces.

Astashev and Babitsky (1998) report that a vibrational frequency during cutting causes a transformation of elasto-plasticity into visco-plasticity [38]. In few words, the dry friction in the contact region between the tool and the workpiece transforms into viscous friction.

VAM is a useful technique to reduce wear in diamond tools. Tool wear can be induced by mechanical-abrasive or chemical-reactive mechanisms. Evans (1999) reports that the unpaired d-electrons are responsible for the chemical-reactive wear mechanism in diamond tools [39]. This reduction in wear takes place due to the following reason. The number of unpaired electrons in the d-orbital of atoms in a workpiece can determine the amount of tool wear during machining. These unpaired electrons enable the breaking of carbon-carbon bonds in the surface of the tool [29]. For instance, Iron has four unpaired electrons, therefore they generate tool wear. Similarly, Nickel and Titanium also cause tool wear and they both have two unpaired electrons. However, copper and aluminium have no unpaired electrons, therefore they don't cause significant tool wear. Another important fact is that low temperature plays a huge role in reducing the reaction rates and this plays a considerable role in reducing the wear rate. In intermittent cutting, the tool is not in contact with the workpiece during most of its vibration cycle so during this period the tool cools down. This temperature drop is known as a potential factor that leads to a decrease in tool wear [29]. Eventually, TWCR plays an important in tool wear. A decrease in TWCR will reduce the temperature during machining, which will lead to a reduction in wear rate. Brinksmeier and Glaebe used elliptical vibration machining to study the relationship between the effective contact time and tool wear. They measure the tool life in terms of the cutting distance at which the surface roughness of the tool dropped below 40 nm (RMS). They report an increase in tool life cutting length from 0 to 20 m when decreasing the effective contact time from 52% to 22% [40].

2.2.3 2D VAM or EVAM principle

Elliptical Vibration Assisted Machining (EVAM) consists of a 2D VAM technique, where the tool is vibrating in 2-dimensions to form an elliptical path. Some of the advantages of this technique are the reversal of the direction of friction and increase in shear angle [41]. The following figure illustrates the motion of the tool during EVAM.

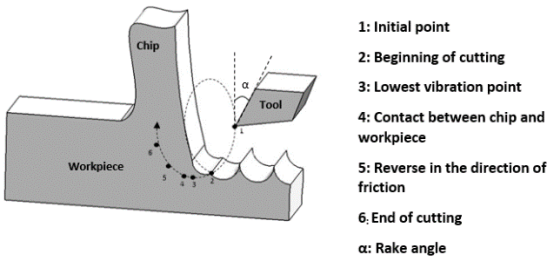

Figure 11 - Illustration of EVAM principle

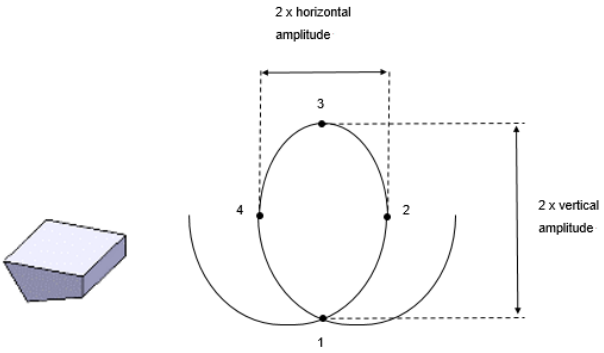

Figure 10 - Tool movement in EVAM

Figure 10 and Figure 11 shows various positions of the tool during the cutting process in EVAM and during this path we can appreciate that the vertical and horizontal vibration velocity vary from zero to a maximum. Table 3 highlights the values of vertical and horizontal vibration velocity of the tool during the elliptical path.

Table 3 - Velocity of the tool at various stages

Position	Horizontal vibration velocity	Vertical vibration velocity
1	Maximum	Zero
2	Zero	Maximum
3	Maximum	Zero
4	Zero	Maximum

Table 4 shows the equations describing the vertical and horizontal displacement of the tool with respect to time and the maximum horizontal and vertical components of velocity of the tool.

Table 4 - Equations of motion in elliptical vibration machining

Variable	Equation
Vertical displacement	$s_y = Bcos(\omega t)$
Horizontal displacement	$s_x = vt + Asin(\omega t)$
Maximum horizontal vibration velocity	$vx_{max} = A\omega$
Maximum vertical vibration velocity	$vy_{max} = B\omega$

Where A is the horizontal amplitude, B is the vertical amplitude, v is the horizontal velocity of the tool and ω is its angular velocity.

The force acting on a tool can be divided into two components. The principal force (or cutting force) and the thrust force. The cutting force is the force involved with plastic deformation to form the chip. The thrust force is related to friction forces and they arise from the contact between the rake face of the tool and the chip. The main advantage of EVAM over VAM is that friction forces are significantly reduced, and this decreases the cutting forces during machining. The reduced friction forces are associated with the vertical vibration velocity of the tool.

In EVAM, during the initial stage of the cutting period, the vertical vibration speed is lower than the speed of the chip flow. This causes friction between the chip and the rake face tool, which consequently leads to the chip being pushed down. However, when the vertical vibration speed of the tool exceeds the speed of the chip flow, it causes the chip to be pulled upwards and this causes an effect known as reversed friction. Shamoto and Moriwaki (1994) report that the average frictional force over many cycles is known to be less than zero “virtually” as the chip is driven by the rake face of the tool [42]. This “reversed friction force” causes lower cutting forces, lower chip thickness, supresses the generation of burrs and enables higher shear angles compared with 1D vibration assisted machining and this is the main advantage of EVAM [43]. During the final stage of the elliptical motion, the tool moves down without cutting, therefore it comes out of contact

with the chip. For instance, Chunxiang et al. (2005) reports that the height of burrs in EVAM is 15 times lower than in VAM when working with Aluminium (52S), which has a significant impact in machining time and cost involved with deburring processes [44].

Interestingly, it has also been reported that increasing amplitude and frequency increases the amount of time that the vibration speed of the tool exceeds the chip flow speed [45]. This can reduce considerably the average frictional force exerted on the chip.

Eiji Shamoto (1994) reports that increasing the frequency of EVAM leads to an increased shear angle [42]. Depending on the size of the ellipse the reduction of cutting forces take place due to distinct reasons. For narrow horizontal ellipse, the reduction in cutting forces is caused by overlapping tool paths. This results in chip thickness being smaller than the depth of cut [46]. In contrast to that, the reduced cutting forces in narrow vertical ellipse takes place due to the tool velocity exceeding the chip velocity, which causes the direction reversal of the friction force acting on the chip and the tool [29].

Once the direction of the tool motion exceeds the shear angle, the velocity of the tool will exceed the velocity of the chip. At this point the friction acting on the chip is assisting its motion instead of opposing it. This causes a significant reduction in heat generation and cutting forces [47].

New frontiers in elliptical vibrational cutting will arise once the high power elliptical vibrators can operate at higher frequencies and higher vibration amplitudes [48]. One of the current research areas is applying EVM at ultrasonic frequencies, which will enable the manufacture of patterns on materials such as aluminium, that can be used as gratings. The challenge is to make a spacing distance between these patterns in the range of 10μm, which requires the use of ultrasonic frequencies. Yang et al. (2016) report notable improvements in this area as they achieved vertical and horizontal amplitudes of 12μm and 4.5μm [49].

2.3 Introduction, applications and limitations of atomic-scale simulation

In this section I will highlight the importance of MD as a simulation tool to study microstructural changes during machining; a special focus will be given to modelling plasticity in materials.

Firstly, I will describe the different simulation techniques that are used to model plasticity, define where Molecular Dynamics sits and its main difference with other simulation techniques. Subsequently, I will explain the analytical framework of MD and ultimately, the limitations of MD as a tool to study large time-scale phenomena and large size-scale systems.

2.3.1 Introduction and applications of atomic-scale simulation

Simulation techniques have played a key role in science as it allows to gain a fundamental insight into conditions that are either too challenging or too costly to study experimentally.

Figure 12 illustrates the types of simulation techniques that are used in the scientific field depending on the length and time scales being studied.

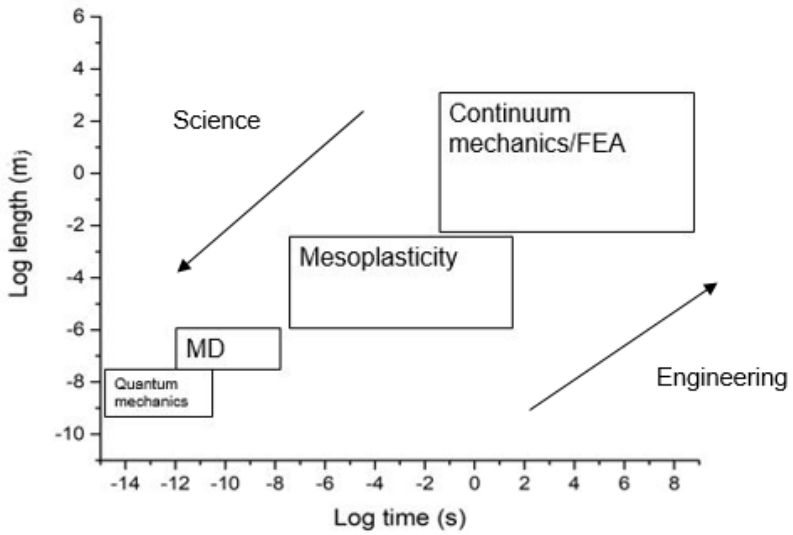

Figure 12 - Simulation techniques in computational materials science

To model the behavior of large-size objects (10 – 10^4 m) the most common approach is to apply continuum mechanics. The scientific field that studies

plasticity at these length and time scales is known as continuum plasticity theory. This technique studies the mechanical behavior of materials by considering them as a continuous mass as opposed to discrete particles. It relies on physical conservation laws, such as the conservation of mass, conservation of momentum and conservation of energy, to derive differential equations that describe the behavior of an object or system. One of the main problems in using this approach to study plasticity is that, although it has proven reliable to study systems in the macro-scale, it has failed to describe plasticity in micro and nano-scale samples. It has been established that materials at macro-scale behave differently to materials at nano-scale [50]. One of the main reasons for this is that the collective motion of dislocations become much more significant at micro and nano-scales; therefore. For instance, size-dependent phenomena such as strain hardening, surface roughening, deformation patterning and fatigue are normally not well described by continuous models of plasticity [51]. Therefore, to describe a material at these small length scales we require computational models that can capture the interaction and movement of dislocation lines.

Mesoplasticity is a fundamental tool to study dislocation dynamics at smaller length scales and the main idea behind this type of simulation is that plastic deformation is governed by the interaction and movement of dislocation lines. Therefore, only dislocation lines have to be considered as opposed to the location and potential of each individual atom in a system so this approach enables length scales of approximately 10 μm and time scales of 1 ms [52]. However, mesoplasticity simulation techniques require the input of several physical models that describe the behavior of dislocation lines, which can be core properties such as line mobility or junction strength. These physical models can either come from experiments or more fundamental simulation tools such as Ab initio molecular dynamics.

There are numerous cases where we need to consider materials as discrete particles. In the case of plasticity in materials, showing the atomic-level details and a quantitative description of how dislocation loops are nucleated and evolve under an applied stress is of critical importance as they enable us to understand mechanisms such as strain hardening from a fundamental level. Apart from this important understanding of plasticity, it can also provide core parameters than

can be used in higher size scale simulation methods and this is the main reason why atomistic simulation plays a key role in materials science and particularly in this thesis. One of the main limitations with atomistic simulation tools is that they are considerably expensive from a computational point of view, so we can only study the physical properties of a single or a few dislocations. This size scale limit might become a problem as macro scale materials have a vast amount of dislocations colliding and interacting with one another, which significantly affect the properties of a material. Nevertheless, at small size-scales MD does provide an essential description of plasticity and in fields such as contact loading, it has enabled an improved understanding of plasticity.in industrially important materials such as silicon or diamond.

There are various categories of atomistic simulation techniques which differ in terms of accuracy and computational cost.

The Ab-initio simulation technique is based on quantum chemistry and solves the electronic Schrödinger equation to calculate physical properties of a system. This type of simulation can reproduce the most accurate behavior of materials; however, it is significantly expensive from a computation point of view and is normally limited to just a few hundreds of atoms and timescales of approximately a few picoseconds. To reduce this computational cost, there have been alternative simulation techniques developed. These techniques are tight-binding and force field techniques.

The tight binding technique is based in electronic band theory and describes the properties of tightly bound electrons in solids. This technique has enabled the study of materials at atomic-scales with good accuracies and has also enabled to increase the number of atoms in the simulation to even millions of atoms [53].

Ultimately, the force field technique is based in semi-empirical potential functions and these potential functions are used to calculate the potential energy of a system of atoms and determine forces acting between them. These potential functions are obtained by analytical approximations to ab initio results and uses experimentally derived empirical parameters. Atoms are treated as point masses and this technique determines the trajectories of atoms by solving Newton’s

equations of motion numerically. Classical molecular dynamics uses the force field approach and is the technique that will be used in our simulation.

In molecular dynamics, the trajectories of atoms obey the Newton's second law, as follows.

$$m_i \frac{d^2\vec{r_i}}{dt^2} = \vec{F_i}(\vec{r_i}, \dots, \vec{r_N}) \tag{3}$$

In the above equation, m_i represents the mass and r_i is the position vector of the i^{th} particle in the system. The potential energy ($U(\vec{r_i})$) of each atom is dependent on its position and the force acting on each atom is the gradient of the potential energy of each atom as shown in the following equation.

$$F = -\nabla U(\vec{r}) \tag{4}$$

Molecular dynamics then makes use of the velocity-verlet algorithm to numerically integrate the equations of motion and hence calculate the position and velocity of each particle at each timestep. Following is the velocity-verlet algorithm that is used.

$$\vec{r}(t + \Delta t) = \vec{r}(t) + \vec{v}(t)\Delta t + \frac{1}{2}\vec{a}(t)\Delta t^2 + \frac{1}{6}\vec{b}(t)\Delta t^3 + O(\Delta t^4) \tag{5}$$

$$\vec{r}(t - \Delta t) = \vec{r}(t) - \vec{v}(t)\Delta t + \frac{1}{2}\vec{a}(t)\Delta t^2 - \frac{1}{6}\vec{b}(t)\Delta t^3 + O(\Delta t^4) \tag{6}$$

By combining both equations, we obtain the following expression.

$$\vec{r}(t + \Delta t) = 2\vec{r}(t) - \vec{r}(t - \Delta t) + \vec{a}(t)\Delta t^2 + O(\Delta t^4) \tag{7}$$

Where, $\vec{r}$ is the position vector, $\vec{a}$ is the acceleration vector and O is the truncation error.

The algorithms just discussed are used to integrate the equations of motion in a system where the total energy is conserved. In many occasions, we may be interested to control the temperature and pressure of a system of particles so that

we can mimic experimental conditions. To model such a system, we can use thermodynamic ensembles that allow us to control state variables such as the energy (E), volume (V), temperature (T), pressure (P) and the number of particles in our system (N). The main thermodynamic ensembles used in molecular dynamics are the NVE. NVT and NPT ensembles.

The NVE ensemble, also known as the microcanonical ensemble maintains a constant energy and volume in the system and results by solving Newton's equation with no temperature and pressure control.

The NVT ensemble is known as the canonical ensemble and maintains a constant temperature and volume in the system. The temperature is controlled by applying temperature scaling algorithms such as the Nose-Hoover or Berendsen thermostats.

The NPT ensemble enables us to control the temperature and pressure in the system. During the use of NPT ensemble, the pressure can be adjusted by adjusting the volume of your system.

The temperature in molecular dynamics is determined by the standard equation in statistical mechanics. This relates the instantaneous temperature to the kinetic energy of atoms.

$$T_{inst} = \frac{2}{g k_B} E_{kin} \tag{8}$$

Where, g is the number of degrees of freedom, E_{kin} is the kinetic energy in the current timestep and k_B is the Boltzmann constant [54].

However, the instantaneous temperature value changes each timestep so an average value over a meaningful number of timesteps is more representative. This can be calculated using the following expression.

$$\langle T \rangle = \frac{1}{N} \sum_n T_{inst}(n) \tag{9}$$

2.3.2 Limitations of molecular dynamics

Molecular dynamics has proven to be a useful tool to study the behavior at atomic-scales, but it does have certain limitations. The main limitations of molecular dynamics are some inaccuracies imposed by the potential function, the small-time scales and the small size scales that can be studied. These limitations are quite important so let us explore them further.

The role of semi-empirical potential functions is to describe how atoms interact with one another and it uses experimentally derived parameters to describe this interaction. Sometimes this may be limiting as the potential functions can only be applied in conditions in which the experiment was done. For instance, some potential functions may be ideal to model certain properties of a specific alloy, but inaccuracies may arise when modelling other physical properties. For this reason, the reliability of a potential function can be debatable if it is used outside the conditions in which it was parameterized. Eventually a detailed understanding of the potential function is essential prior to analyzing certain properties of interest.

Timesteps in molecular dynamics should be short enough to capture significant changes that take place at atomic-scales. Often, these timesteps are of the order of a few femtoseconds. Experimentally we tend to look at the evolvement of a system that can take nanoseconds, microseconds or longer so a substantial number of timesteps are needed to completely model these events. This takes a large amount of time and is expensive from a computational point of view; therefore, simulations in molecular dynamics are limited to several hundred picoseconds. This limitation in time scale can have a considerable effect in studying various mechanisms. For instance, when modelling a tensile test very high strain rates must be applied to study the full behavior of materials from their elastic response to fracture in just a few hundred picoseconds.

2.3.3 Comparing EAM and 2NN MEAM interatomic potential functions

In this section, we will consider two potential functions that are commonly used to model metal alloys in molecular dynamics. These potential functions are the Embedded Atom Method (EAM) and the Second Nearest Neighbours Modified Embedded Atom Method (2NN MEAM).

Several semi-empirical potential functions have been developed to describe a wide range of elements and alloys. Some of these potentials are Embedded Atom Method (EAM), Finnis-Sinclaire, Glue and Tersoff [55].

One of the most widely used interatomic potential functions is the EAM potential. EAM provides a function for the energy required to embed an atom in the background electron density generated by the neighbor atoms and it is useful mainly for pure metallic systems that have no directional bonding. The following equation describes the potential energy of an atom i using the EAM interatomic potential function.

$$\bar{\rho} = \sum_{j(\neq i)} \rho(r_{ij}) \tag{10}$$

$$E = \sum_{i} E_i = \sum_{i} F(\bar{\rho}_i) + \frac{1}{2} \sum_{ij(i \neq j)} \emptyset(r_{ij}) \tag{11}$$

In this equation, E is the total energy of the system of atoms, F is the embedding function, $\bar{\rho}_i$ is the total electron density at atom i and $\emptyset(r_{ij})$ is the interaction energy between atom pairs I and j [56].

An important limitation in these potential functions is that they can't model a wide range of crystal structures. Therefore, it becomes difficult to model metallic systems with different elements and crystal structures using a single framework [55]. For instance, the EAM potential function doesn't account for directional bonding therefore, it inaccuracies may arise when modelling non-fcc metals [57].

To overcome this limitation, an additional interatomic potential function was developed called the Modified Embedded Atom Method (MEAM). The MEAM interatomic potential function has proven suitable to accurately model a wide range of crystal structures using one single formalism.

The MEAM potential is an extended version of EAM and it accounts for directional bonding and special arrangements of neighboring atoms [58]. Initially, the MEAM potential only considered interactions between first near-neighbor atoms. However, in certain crystal structures such as bcc, the second nearest neighbor

distance is only ~15% larger than the first near neighbor distance [55]. Therefore, the second nearest neighbor should not be completely negligible. There have been recent improvements done on the MEAM potential by Lee and Baskes [59] and Lee et al [60]. This new potential is called 2NN MEAM and the improvements allow interactions between second nearest-neighbor atoms. There has been a significant amount of work done using 2NN MEAM to model a wide range of alloys; however, it hasn't been used extensively to model shape memory alloys, particularly CuZr shape memory alloy. For this reason, one of the aims of this thesis is to evaluate whether the 2NN MEAM potential is suitable to model the physical properties of Cu-Zr shape memory alloy and whether it can provide an insight into the microstructural changes of this material during machining. The following equation describes the potential of energy of a system of atoms using the 2NN MEAM interatomic potential function [61].

$$E = \sum_{i} F_i(\overline{\rho}_i) + \frac{1}{2} \sum_{i.j(j\neq 1} S_{ij} \emptyset_{ij}(R_{ij}) \tag{12}$$

F_{ij} denotes the energy that an atom i obtains when embedded in an electron density ρ_{ij}.

$\emptyset_{ij}$ represents the pair interaction between atoms i and j and S_{ij} is the degree of screening on the interaction between atom i and j by neighbouring atoms.

3 METHODOLOGY

3.1 Evaluating the choice of potential function

In the thesis, the EAM was compared to the 2NN MEAM interatomic potential functions to determine which is the most optimum potential function to be used. In MD, the general approach to test the reliability of a potential function to model the mechanical properties of a material is to calculate its elastic constants, lattice parameter and cohesive energy and compare these results with first principles. The way these properties are calculated is as follows.

To make this comparison, the energy of the B1 and B2 crystal structures of CuZr binary alloy was minimized to find their lowest energy conformation (where the net interatomic force on each atom is close to zero). This enabled us to determine its optimized structure. To perform this task, molecular dynamics iteratively adjusts the atomic coordinates until a local minimum potential energy configuration is obtained. Once the optimum atomic configuration of each crystal structure is obtained, their corresponding lattice parameter, cohesive energy and bulk modulus at 0K using each potential function is calculated. Ultimately, these results are compared with first principles calculations from the literature to establish which potential function gives the best approximation.

3.2 Tensile and shear test simulation

To run the tensile test simulation for each of the phases CuZr, $CuZr_2$ and Cu_5Zr, a nanowire of length 34.4nm and diameter 12.3nm was constructed with the crystal orientation and direction of tensile pulling as <010>. Periodic boundary conditions were set in the x, y and z directions. The nanowire followed NVE dynamics and was initially equilibrated at 10K using a timestep of 0.5 fs. A strain rate of 0.0005 ps^{-1} was applied to the sample.

The stress acting on the specimen was derived by calculating the pressure of the entire system of atoms in the y-axis. The computed pressure in in units of bars, hence dividing this value by 10000 gave us pressure units in GPa.

In addition, the LAMMPS command stress/atom was used to compute the stress tensor on each atom; however, the computed quantity is in units of pressure x

volume. For this reason, the computed quantity would need to be divided by a per-atom volume to have units of stress. Atomic volume can be obtained by simply computing the volume of your sample and dividing this value by the number of atoms composing the sample.

$$Stress = \frac{Computed\ stress/atom}{Atomic\ volume} \tag{13}$$

To apply the strain rate, the LAMMPS command fix deform was used. This command changes the volume or shape of the simulation box to model systems that are continuously strained. By using this command, the simulation box size changes according to the following equation.

Where $L(t)$ is the length of the simulation box (in the strain direction) as a function

$$L(t) = L_0(1 + erate \times dt) \tag{14}$$

of time, L_0 is the initial length of the simulation box, erate is the applied engineering strain rate and dt is the elapsed time (timestep).

3.3 Machining

To run the nanocutting simulation, a cylindrical nanowire was built and was made to rotate about the vertical axis (z-axis). The way the workpiece was made to rotate is as follows. The cylindrical nanowire was divided in two sub-sections. The first section consists a central region of the nanowire (up to a radius of 7.1 nm) and the core atoms in this region were made to rotate about the z-axis. The outer most region is composed of Newtonian atoms, which follow NVE dynamics and atoms in this region were driven to rotate due to the movement of the core atoms. The stress in the 1 nm^3 region was calculated as follows. The stress/atom command in LAMMPS enables us to compute the symmetric stress tensor of each individual atom in the 1 nm^3 region; hence, adding the appropriate components of stress acting on each atom within this region enabled us to calculate the stress tensor in the 1 nm^3 region and consequently the Von mises, Tresca and maximum principle stresses acting in that region.

The tool was modelled as a rigid object composed of CuZr (same composition as workpiece) and was made to move with elliptical vibration motion. Figure 13 and Table 5 show an illustration of the machining set up and the parameters implemented Table 5

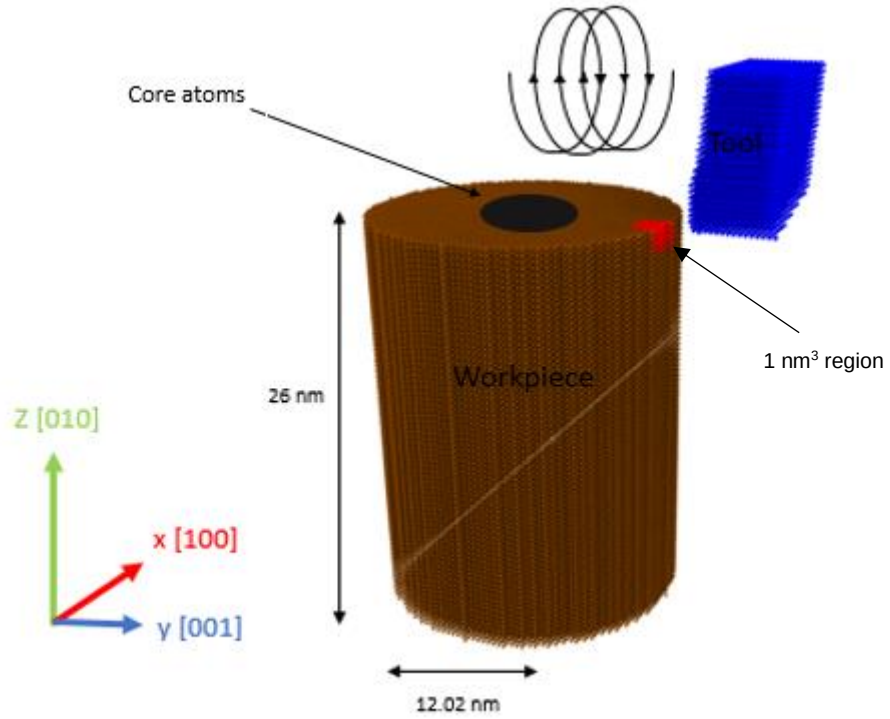

Figure 13 - EVAM simulation

Table 5 - EVAM parameters

Parameters	Values
Workpiece dimensions	Radius: 12.02 nm Length. 26 nm
Number of atoms	692003
Cutting direction	[010]
Tool rake angle	35º
Tool clearance angle	20º
Cutting distance	10 nm

Nominal cutting speed of the tool	6 nm/ps
Workpiece rotation (RPM)	$5x10^{11}$ RPM
Vibration frequency	3.3×10^{11} Hz
Vertical amplitude	1 nm
MD timestep	0.0005 ps
Total simulation time	200 ps

4 RESULTS

4.1 Comparison between EAM and 2NN MEAM potential

To establish the optimum potential function to be used in this simulation we compared EAM and 2NN MEAM potential functions.

An energy minimization was carried out for the B1 and B2 crystal structures of Cu-Zr and subsequently the lattice parameter and bulk modulus of each crystal structure was calculated at 0K. We then compared these results with first principles data. The following table summarizes the results.

As can be observed the 2NN MEAM potential gives a higher approximation to first principle data in comparison with EAM potential. For this reason, the 2NN MEAM potential was considered as the optimum potential to be used in this simulation.

$$C_{11} = C_{22} = C_{33}$$

$$C_{12} = C_{13} = C_{23}$$

$$C_{44} = C_{55} = C_{66}$$

$$Voigt\ Bulk\ Modulus = \frac{(C_{11} + C_{22} + C_{33}) + 2(C_{12} + C_{13} + C_{23})}{9} \qquad (15)$$

Table 6 - Comparison of EAM and 2NN MEAM potential with first principle results

Crystal Structure	**Parameter**	**EAM**	**2NN MEAM**	**First Principles results (Gosh, 2007)** [62]
B1	Lattice parameter at 0K (Å)	5.126	5.344	5.343
	Voigt Bulk modulus at 0K (GPa)	85.89	76.52	76.6
B2	Lattice parameter at 0K	3.228	3.250	3.259
	Voigt Bulk modulus at 0K (GPa)	124.3	119.3	121.4
	Shear modulus (GPa)	41.56	41.42	43.2 [63]

4.2 Lattice parameter of 6 phases of Cu-Zr binary system at 0K

The lattice parameter and bulk modulus was calculated for 6 phases of the Cu-Zr binary system using the 2NN MEAM interatomic potential function and the results were compared with first principle. The results are summarized in tables 2 and 3.

Table 7 - Lattice parameter of 6 crystal structures of CuZr binary system using the 2NN MEAM potential function

Crystal structure	Lattice parameter (2NN MEAM result)/Å	Lattice parameter (First principles)/Å (Gosh, 2007) [62]
B1 CuZr	5.344	5.343
B2 Cu-Zr	3.250	3.259
$L1_2$ Cu3Zr	3.880	3.933
$L1_2$ CuZr3	4.320	4.283
$C11_b$ CuZr2	3.232 (a)	3.220 (a)
	3.232 (b)	3.220 (b)
	11.22 (c)	11.18 (c)
Cu5Zr F-43m	6.888	6.912

Table 8 - Comparison of 2NN MEAM with first principles data for the bulk modulus of 6 phases of Cu-Zr binary system

Crystal structure	Voigt Bulk modulus (GPa), 2NN MEAM results	Voigt Bulk modulus (GPa) (First principles) (Gosh, 2007) [62]
B1 CuZr	76.5	76.6
B2 CuZr	119.35	121.4
$L1_2$ Cu3Zr	96.78	118.8
$L1_2$ CuZr3	100.9	99.8
$C11_b$ CuZr2	107.96	112.1
Cu5Zr F-43m	136.86	139.2

4.3 Tensile test results

The tensile test simulation was conducted for the B2 CuZr, C11b $CuZr_2$ and Cu_5Zr phases. Figure 14 shows the dimensions of the Cu-Zr nanowire.

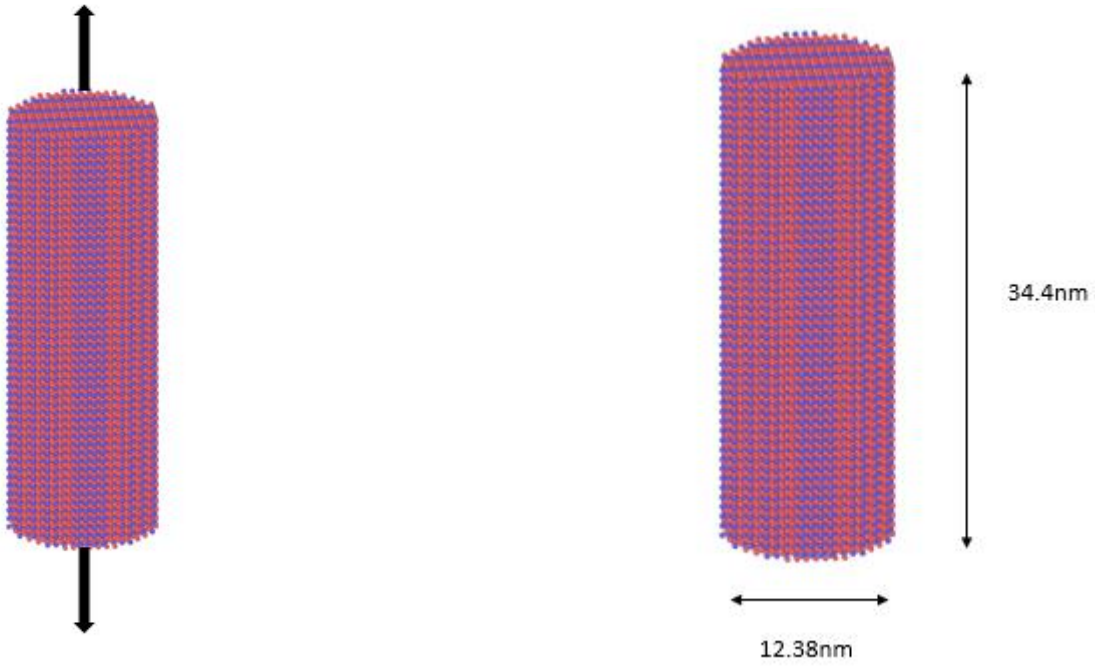

Figure 14 - Dimensions of the nanowire for the tensile test

Figure 15 illustrates a section of the nanowire at various stages of its deformation.

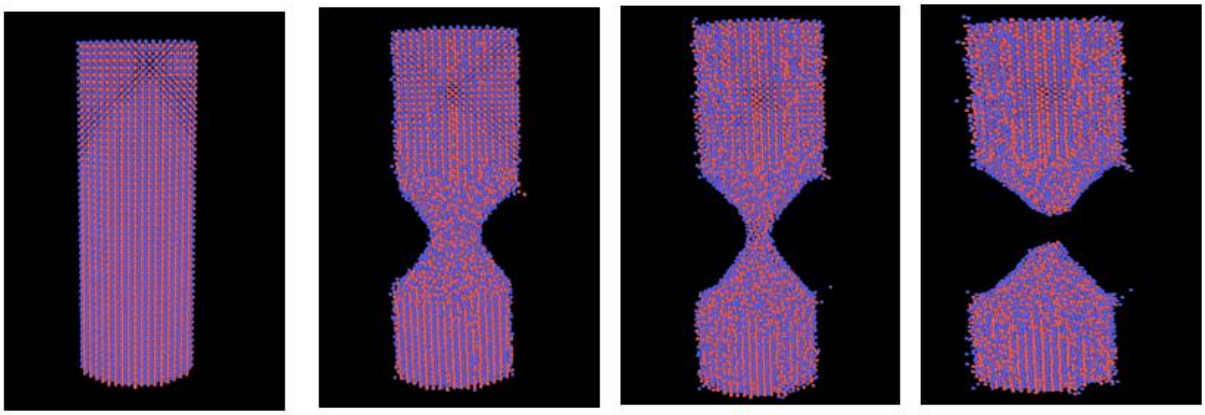

Figure 15 - Snapshots of the Cu-Zr (B2) nanowire during the tensile test

Common neighbor analysis (CNA) is a tool used in visual molecular dynamics and its main purpose is to identify the phases present in a sample. CNA uses characteristic signatures from the topology of bonds to match a local structure to an idealized one (such as FCC or BCC) and measures how closely they fit. This

information is then used to colour particles according to the crystal structure they belong to for visualization purposes. In this work, this enables us to study the phase changes that take place during deformation. Figure 16 shows a representation of colour coding used in the CNA tool to identify particles corresponding to different crystal structure.

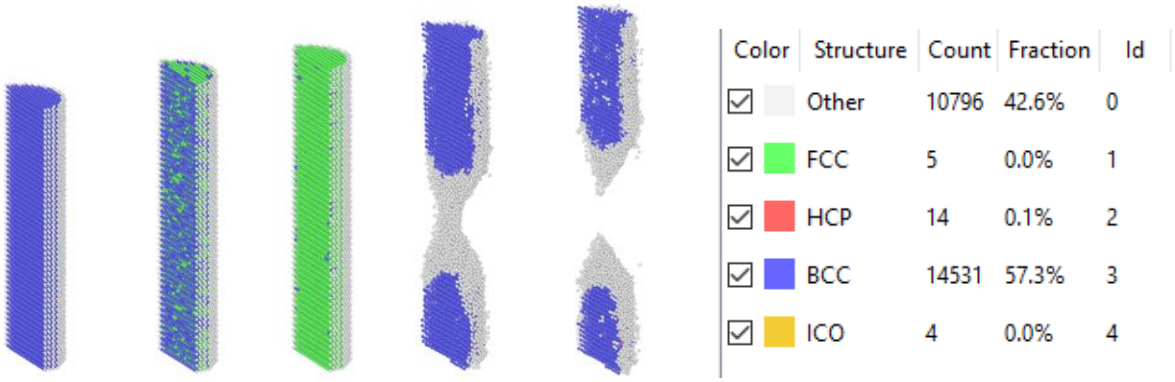

Figure 16 - Use of CNA to evaluate phases present during the tensile test of Cu-Zr binary system

Figure 17 shows the results obtained for tensile test simulation for three different compositions of Cu-Zr.

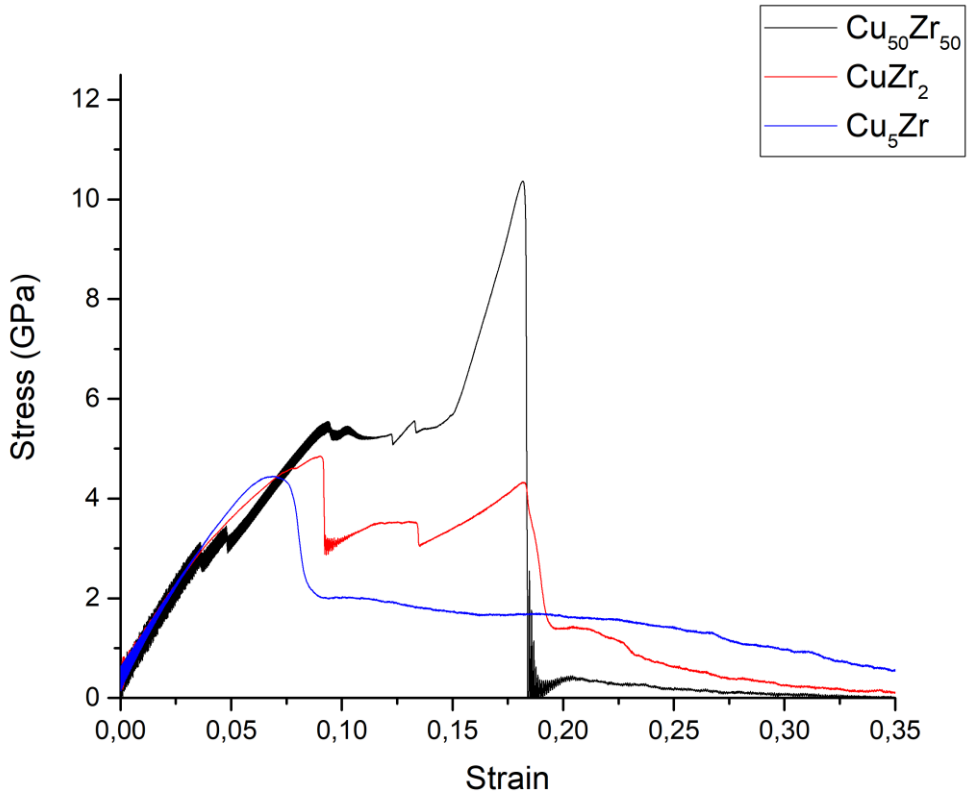

Figure 17 - Tensile test results for the Cu50Zr50, CuZr2 and Cu5Zr crystal structures

Although different metals have different properties, the stress-strain relationship in metals generally show some common characteristics. For instance, we normally observe a linear stress-strain relationship up until a well-defined yield point. Upon further loading the metal plastically deforms and does not return to its initial length when the stress removed.

Interestingly, we can appreciate this type of stress-strain relationship in the Cu_5Zr phase. However, the phases $Cu_{50}Zr_{50}$ and $CuZr_2$ show a different type of stress-strain relationship.

The drops in stress for the compositions $Cu_{50}Zr_{50}$ and $CuZr_2$ are due to a behaviour known as pseudoelastic effect, which is an elastic response caused by a diffusionless phase transformation when a stress is applied. This type of behaviour has been studied extensively as it is a characteristic feature of smart materials known as shape memory alloys. The main advantage is that it allows the material to undergo large and reversible amounts of strain.

Figure 18 and Figure 19 shows loading and unloading stages for $Cu_{50}Zr_{50}$.

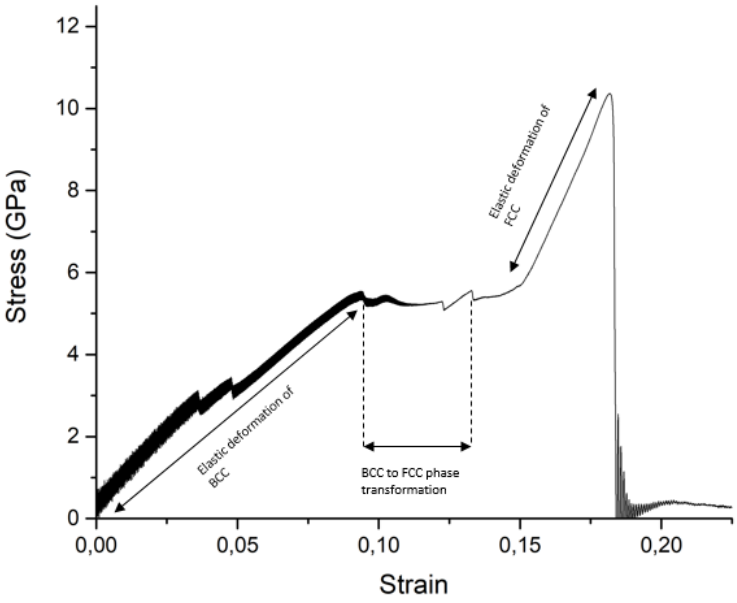

Figure 18 - Stress-strain curve of CuZr binary alloy

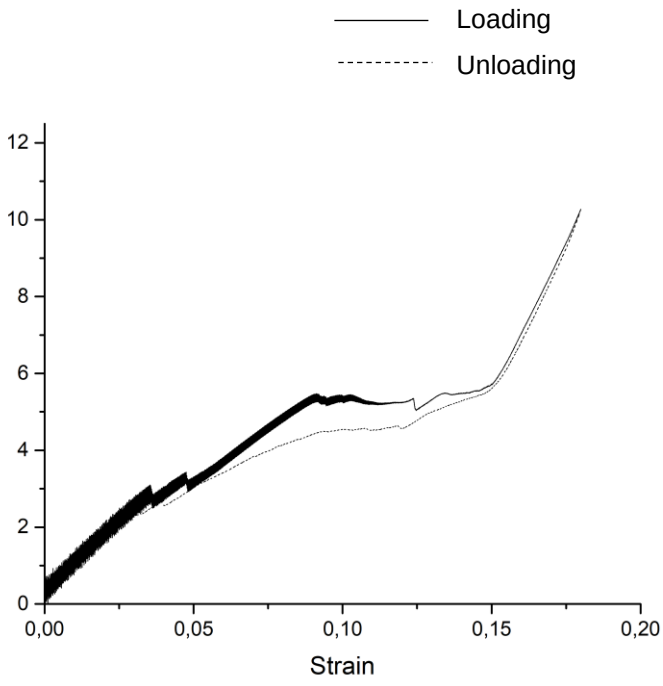

Figure 19 - Loading and unloading curves in CuZr binary alloy

The initial deformation stage from A to B corresponds to the elastic deformation of the B2 crystal structure. We can also appreciate serrated behaviour at this initial stage of the simulation, which is caused by thermal fluctuations in the sample. These thermal fluctuations may be due to non-stabilized thermal equilibration during the initial deformation stage. However, it decreases significantly as it approached the critical stress of phase transformation. Another interesting feature in the graph is first drop in stress highlighted in figure 12. Recent reports suggest this stress drop and change in young's modulus to be related to the non-linearity of the potential function, which may be a potential cause as there are no phase transformation taking place and there is perfectly elastic behaviour.

The elastic deformation reaches a critical stress of 5.42 GPa at point B. At this critical stress, there is a diffusionless phase transformation from B2 to B19' (austenite to martensite) and this observed from B to C in the stress-strain graph. During this stage, there is an increase in strain with no substantial increase in

stress. The phase transformation is complete at a strain of 0.146. Upon completion of the phase transformation, the elastic deformation of martensite takes place.

The martensitic elastic deformation is represented by the second linear region in the stress-strain graph from C to D. The stress at point D is 10.35 GPa, which agrees remarkably well with previous MD simulations of Cu-Zr pseudoelasticity using the EAM potential [64]. At this point, yielding of B19' takes place at a strain of 0.181, which is shown by nucleation and propagation of dislocations, ultimately leading to fracture. The maximum recoverable strain is 0.181.

During the phase transformation, we can also observe a serrated curve. This serrated curve during a phase transformation has been reported previously, so a few behaviours may explain this phenomenon. One of the explanations may be related to the stress-induced martensitic deformation occurring in regions with localized bands of plastic deformation, known as Lüders bands and has been previously observed in NiTi alloys [65].

The Young's Modulus of the first linear region is 72.26 GPa, the second linear region is 57.8 GPa. Saitoh et al. (2009) suggests that this drop in stress is due to the non-linearity of the potential function [66]. The Young's modulus of the martensite structure is 154.97 GPa.

The red line corresponds to the unloading stage. The main reason to evaluate this unloading stage is to conclude whether there is a hysteresis loop being formed. Studying the hysteretic response of shape memory alloys is of great importance as it provides energy dissipating and damping capabilities for structural vibration control in aerospace applications [67].

Song et al. (2007) performed experiments to test the martensitic transformation in CuZr metallic glass reinforced with B2 crystal phases. This study reports that the phase transformation from B2 to B19' (martensite) takes place at a critical stress of 1500 MPa [68], which is considerably lower to what has been observed in our simulation. Although these tests were not performed with single crystal B2 structures and the sample size was considerably larger than the one used in our simulation, we may observe a significant difference in critical stress, but it does

provide a clear correlation with our simulation in terms of the phase transformation taking place. Furthermore, Cheng et al. (2009) performed MD simulations to study the critical stresses of B2 to B19' phase transformation and unloading behaviour in B2 CuZr nanowires at different temperatures. His findings showed that at 50K the B2 to B19' phase transformation takes place at a stress of 6 GPa and the strain for which the phase transformation is complete is 0.4, which agree well with our simulation [64].

Figure 20 shows snapshots of martensite nucleation at strains of 0 (100% b2), 0.09627 (87.2% b2 and 3.6% martensite at step 385000), 0.112 (56.5% b2 and 34.3% martensite step 450000) and 0.16 (0.1% b2 and 90.4% martensite step 640000). Blue atoms correspond to a b2 crystal structure and green atoms correspond to the B19' crystal structure.

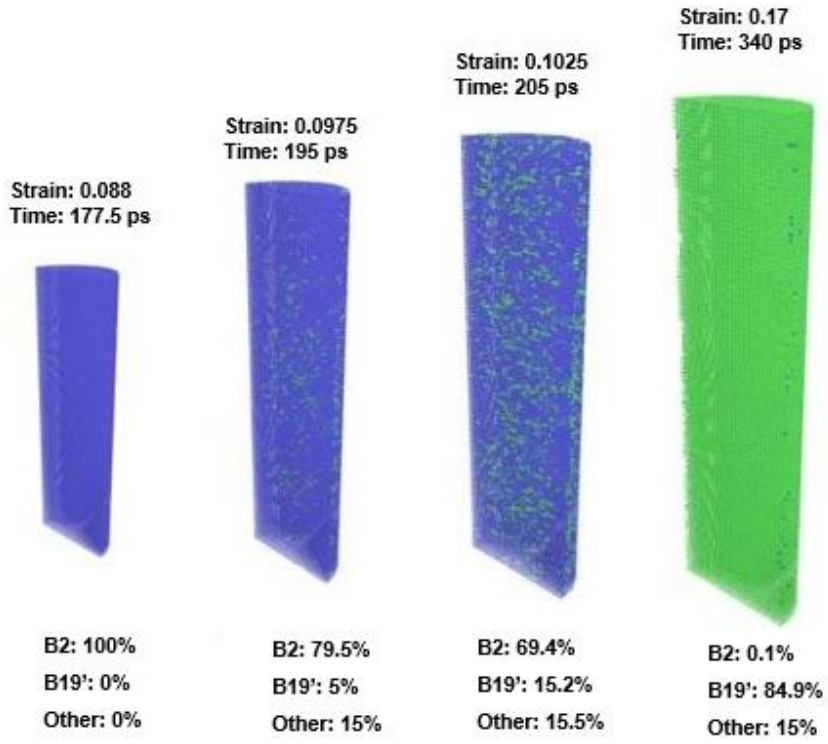

Figure 20 - Phase transformation illustration in Molecular Dynamics

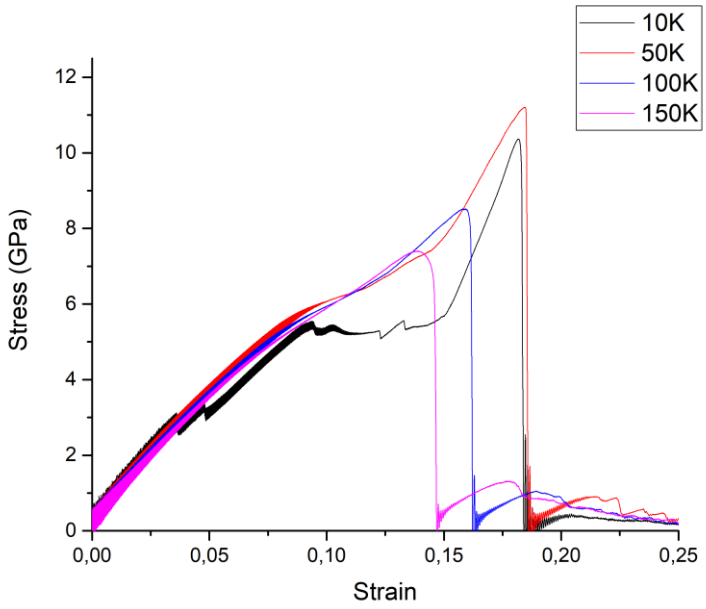

Figure 21 - Stress vs strain curve for B2 Cu-Zr binary alloy at 10K, 50K, 100K and 150K

Table 9 - Comparison of mechanical properties of the B2 Cu-Zr crystal structure at 10K, 50K and 100K

	10K	**50K**	**100K**
Young's modulus (GPa)	73.1	67.6	65.5
Maximum recoverable strain	0.181	0.182	0.158
Critical stress for phase transformation (GPa)	5.30	5.71	5.77

Figure 21 shows the stress-strain curve of the B2 crystal structure at 10K, 50K, 100K and 150K. The graph clearly shows that as the temperature is increased the critical stress required to induce a phase transformation also increases. It is argued that the critical stress at which austenite transforms into martensite increases as temperature increases. This happens because at higher

temperatures the stability of the austenite phase increases. For this reason, an increase in stress is required so that the mechanical energy exceeds the high thermodynamic stability of the austenite phase [69]. It can also be observed that increasing the temperature above 10K enables a smoother phase transformation without serrated behaviour in comparison with the tensile test at 0K.

In our simulation, the b2 CuZr crystal structure showed pseudoelastic behaviour across the temperature range 10K to 150K. As complementary information, the literature suggests that there is a temperature (which hasn't been tested in this thesis) above which austenite does no longer transform in martensite under deformation. This takes place due to the dislocation slip of austenite [70]. It is important to highlight that the critical stress of martensitic transformation increases with temperature and the critical stress at which dislocation slip takes place decreases with temperature. The point in which these two critical stresses meet is the temperature above which martensitic transformation can no longer occur [70] so there is a limit in temperature above which phase transformation is not observed. Further study of dislocation slip resistance is significantly important to determine whether pseudoelasticity or dislocation mediated plasticity will take place in a material during deformation.

The C11b structure does show a peculiar stress-strain relationship; however, it hasn't been studied further in this thesis. Interestingly, Cu_5Zr doesn't show phase transformation during its tensile test. After its elastic region it shows very small plastic deformation before fracture.

4.4 Shear test

Figure 22 shows the shear test results for three phases of Cu-Zr binary alloy.

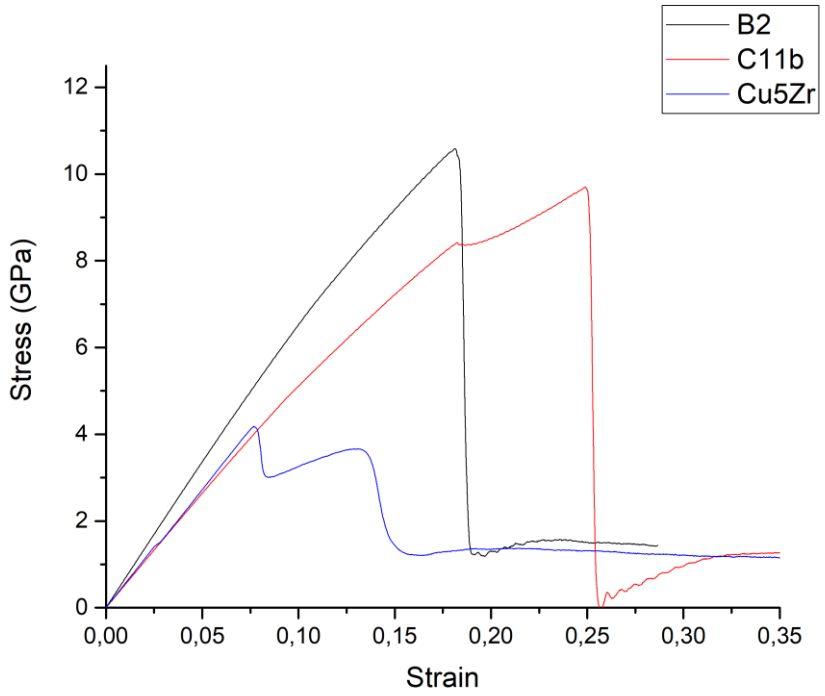

Figure 22 - Shear test results for three phases of Cu-Zr binary alloy

Table 10 - Shear properties for three phases of Cu-Zr binary alloy

	B2	**C11b**	**Cu_5Zr**
Shear Modulus (GPa)	67.27	51.98	52.83
Shear strength (GPa)	10.57	9.57	4.16

Interestingly, we can observe a stress drop on the C11b crystal structure at a strain of 0.18. The use of CNA via OVITO enabled us to identify that there is a phase transformation taking place at this point. Similarly, this is observed in the Cu_5Zr crystal structure, at the point where a significant stress drop is observed at a strain of 0.077.

4.5 Conventional machining and elliptical vibration assisted machining

4.5.1 Conventional machining

Figure 23 and table 11 shows the variation of cutting forces with time and the peak stresses in conventional machining.

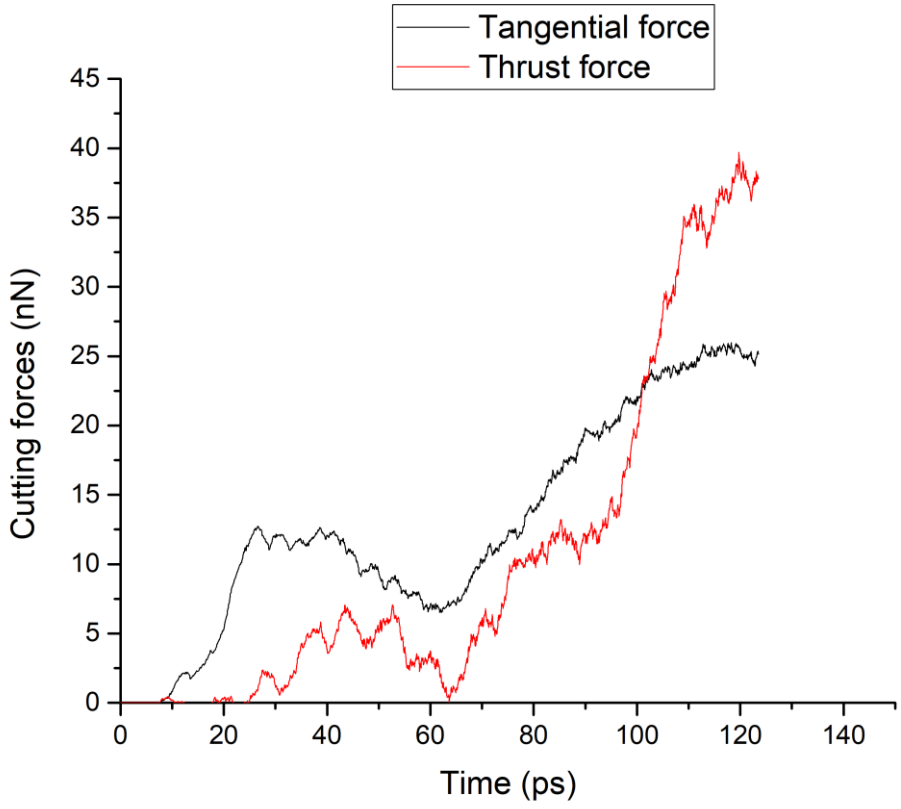

Figure 23 - Cutting forces in conventional machining

Table 11 - Average cutting forces and peak stresses during conventional machining

Average cutting forces	
Tangential force	12.70 nN
Thrust force	14.59 nN

Stress peak causing nanoscale yielding	
Von Mises stress	16.16 GPa
Tresca stress	8.75 GPa
Maximum principal stress	16.74 GPa

4.5.2 Elliptical vibration assisted machining

Figure 24 and table 12 shows the variation of cutting force with respect to time and peak stresses during EVAM.

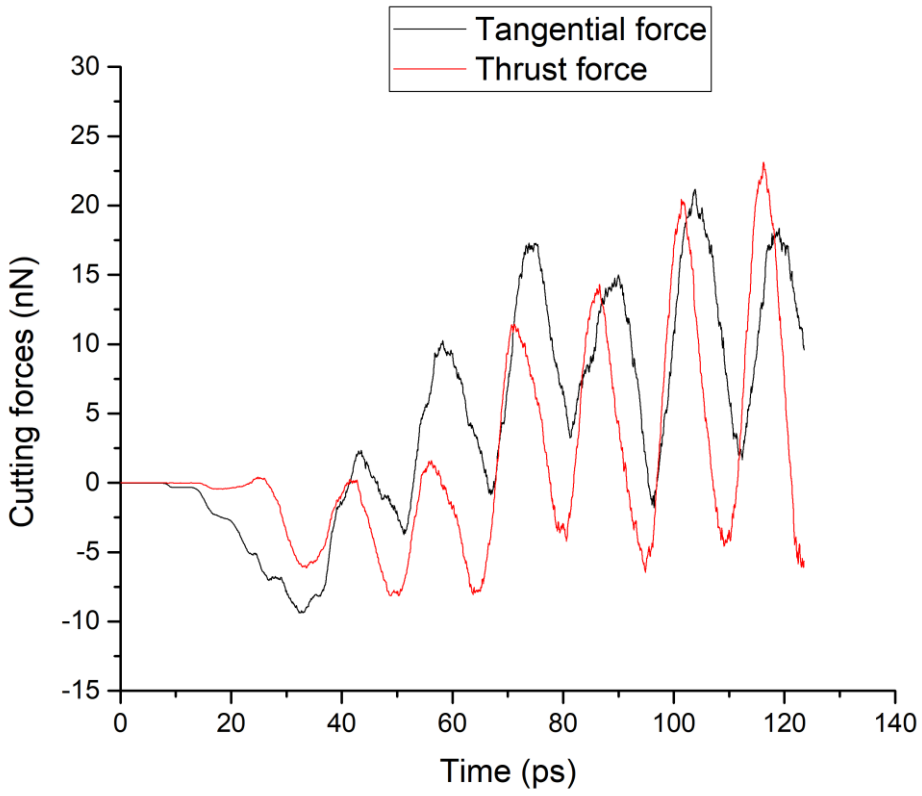

Figure 24 - Cutting forces in EVAM

Table 12 - Average cutting forces and peak stresses during EVAM

Average cutting forces	
Tangential force	5.00 nN
Normal force	2.14 nN

Stresses during machining	
Von Mises stress	17.3 GPa
Tresca stress	9.56 GPa
Maximum principal stress	22.13 GPa

Figure 25 and figure 26 shows the comparison of tangential force and cutting force between EVAM and conventional machining of CuZr SMA.

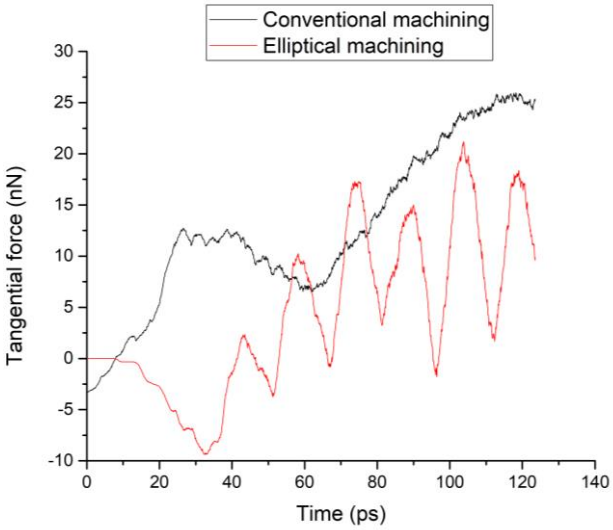

Figure 26 - Comparison of tangential force during conventional machining and EVAM of CuZr SMA

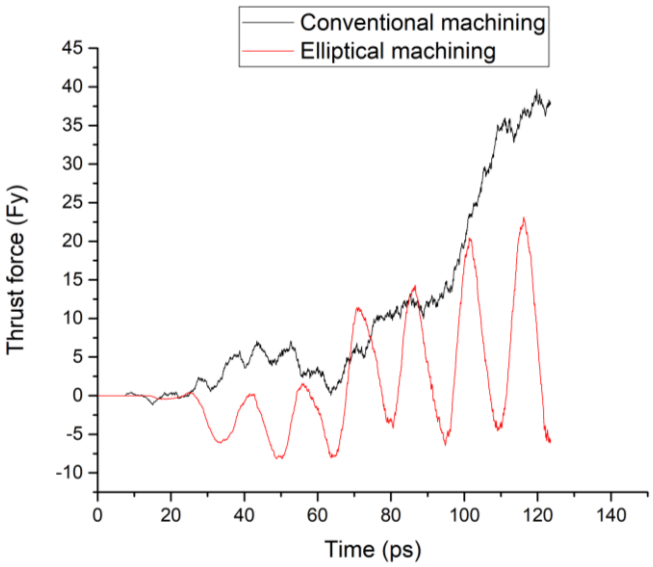

Figure 25 - Comparison of thrust force during conventional machining and EVAM of CuZr SMA

We can appreciate that EVAM shows lower tangential and normal forces during machining compared with conventional machining and the stresses don't vary much between the two techniques.

The polyhedral template matching (PTM) in OVITO was used to identify the localised crystal structure of atoms. This algorithm is used in the presence of high strain and thermal fluctuations as it offers greater reliability than CAN under these conditions. The dislocation extraction algorithm (DXA) from the Crystal Analysis Tool (CAT) was used to identify the types of dislocations present during the machining simulation. The results showed that there was no dislocation nucleation or martensitic transformation during both types of machining. Instead, amorphisation was the primary plastic mechanism observed in both techniques. Amorphisation is defined as the change of a crystalline material to one with an amorphous (or disordered) microstructure. The amorphisation process in materials has been extensively studied and can normally be obtained by ion irradiation, rapid quenching from the melt or at high strain-rate loading.

5 DISCUSSION

Different behaviors have been observed for different compositions of CuZr binary alloy in different loading directions. Mechanical characterization of CuZr SMA has shown evidence of pseudoelastic behavior during tension loading for the compositions $Cu_{50}Zr_{50}$ and Cu_2Zr but not for Cu_5Zr. In contrast to that, loading in shear showed pseudoelastic behavior only in the composition Cu_5Zr; hence, loading direction and chemical composition plays a key role in whether pseudoelastic behavior is observed in CuZr binary alloy.

The machining results show a reduction in cutting forces in EVAM compared to conventional machining; however, the stresses on the workpiece were slightly higher in EVAM than in conventional machining. No difference in plasticity was observed between both techniques. No dislocation nucleation and no austenite to martensite phase transformation took place in either of the machining techniques. Instead, the mechanism governing the plastic deformation for both EVAM and conventional machining was amorphisation. Amorphisation has a metastable nature and has been observed during strong mechanical deformation in several materials; therefore, the high strains applied in this simulation may account for this phase change during machining.

As a conclusion, there were some indications that EVAM improved the machinability compared with conventional cutting although this improvement was not significant. However, the fact that no difference in plasticity was observed in both techniques may be a consequence of not running the simulation for a longer period or perhaps not cutting enough length to observe a difference in plastic deformation mechanisms. These factors can be evaluated further in future work.

A clear observation is that the mechanism of amorphisation is competing against dislocation nucleation and martensitic transformation during the deformation process. The explanation to this is that in different loading directions, the critical resolved shear stress to cause phase transformation, dislocation or amorphisation is different. Hence, the preferred plastic deformation mechanism in a specific loading direction will be the one requiring the lowest critical resolved shear stress.

6 CONCLUSIONS

In this thesis we have characterized the mechanical properties of CuZr during a tensile and shear test and evaluated the nanoscale material removal mechanism of CuZr SMA during EVAM. Let us summarize the main conclusions of this research.

In connections with the mechanical characterization of CuZr SMA we have arrived at the following conclusions. Tensile test, shear test and machining were carried out in MD and we have observed phenomena such as pseudoelasticity, dislocation nucleation in the austenite phase and amorphisation. In the tensile test simulation, the load was applied in the crystal direction <010>, and the phases $Cu_{50}Zr_{50}$ and Cu_2Zr showed pseudoelastic behavior during loading whereas the phase Cu_5Zr showed dislocation nucleation prior to fracture, therefore no pseudoelastic behavior was observed. In contrast to that, the shear test showed pseudoelastic behavior in the Cu_5Zr phase, but no phase transformation was observed in the $Cu_{50}Zr_{50}$ and Cu_2Zr phases.

Tensile test was carried out on the b2 CuZr crystal structure at different temperatures and the results showed pseudoelastic behavior across the temperature range 10K to 150K. The main outcome is that the critical stress for phase transformation increased as temperature increased, agreeing well with Clausius-Clapeyron relationship.

As far as machining is concerned, the machinability achieved by EVAM is not substantially better than conventional machining. The cutting forces in EVAM were lower than in conventional machining but the stresses where slightly higher in EVAM. Furthermore, no difference in plasticity was observed between the two techniques. During both, conventional machining and EVAM, CuZr SMA experienced amorphisation and no dislocation nucleation or martensitic transformation was observed. This provides evidence that in the cutting direction {100} and at high strain rates, the critical resolved shear stress to cause amorphisation is lower than the critical resolved shear stress to cause dislocation nucleation or martensitic transformation.

7 FUTURE WORK

This work has focused mainly in the outcomes arising from the mechanical characterization of CuZr SMA and machining. Clearly, we have observed that applying the load in different crystal directions yields different microstructural behavior in CuZr binary alloy.

To further explore this difference in behavior, it would be useful to provide a quantitative and more detailed description of why these plasticity responses take place. Calculating the critical resolved shear stress (CRSS) required to induce a martensitic transformation, dislocation slip in the austenitic structure and amorphisation in different loading directions would give us a clear picture of the competition between these three forms of plastic deformation during loading. Several guidelines can be used to calculate these critical resolved shear stresses using atomistic simulation. Material properties such as the generalized stacking fault energy (GSFE) and the generalized planar fault energy (GPFE) enable us to calculate the CRSS to cause dislocation slip in the austenite phase and to cause martensite twinning. Providing this detailed description of behavior would augment our fundamental understanding of the preferred mechanism of plasticity during loading of CuZr SMA.

An additional point to consider is that the strain rate during chip formation was significantly high and the cutting distance was very low in this simulation compared to what is normally seen experimentally and both strain rate and cutting distance may play a key role in the plastic behavior of materials. For this reason, it would be interesting to further study the plastic behavior of CuZr SMA during EVAM and conventional machining simulations with lower strain rates or perhaps a higher cutting distance. Although this may be more expensive from a computational point of view, it may yield some key differences between both techniques that haven’t been observed in this thesis.

8 REFERENCES

[1] K. Saitoh and K. Kubota, “Atomistic simulation on the relation between amorphization and crystalline transformation in Ni-Ti alloy,” *J. Solid Mech. Mater. Eng.*, vol. 4, no. 7, pp. 1061–1070, 2010.

[2] M. Morakabati, S. Kheirandish, M. Aboutalebi, A. K. Taheri, and S. . Abbasi, “A study on the hot workability of wrought NiTi shape memory alloy,” *Mater. Sci. Eng. A*, vol. 528, no. 18, pp. 5656–5663, 2011.

[3] W. Gao, X. Yi, B. Sun, X. Meng, W. Cai, and L. Zhao, “Microstructural evolution of martensite during deformation in Zr 50 Cu 50 shape memory alloy,” *Acta Mater.*, vol. 132, pp. 405–415, 2017.

[4] P. S. Lobo, J. Almeida, and L. Guerreiro, “Shape memory alloys behaviour: A review,” *Procedia Eng.*, vol. 114, pp. 776–783, 2015.

[5] M. Tahara, N. Okano, T. Inamura, and H. Hosoda, “Plastic deformation behaviour of single-crystalline martensite of Ti-Nb shape memory alloy,” *Nature*, vol. 7, 2017.

[6] Y. Aydogdu, A. Aydogdu, and O. Adiguzel, “Self-accomodating martensite plate variants in shape memory CuAlNi alloys,” *J. Mater. Process. Technol.*, vol. 123, no. 3, pp. 498–500, 2002.

[7] K. K. Alaneme and E. A. Okotete, “Reconciling viability and cost-effective shape memory alloy options - A review of copper and iron based shape memory metallic systems,” *Eng. Sci. Technol. Int. J.*, vol. 19, no. 3, pp. 1582–1592, 2016.

[8] M. Bahrami Nasab and M. . Hassan, “Metallic biomaterials of knee and hip - A review,” *Trends Biomater. Artif. organs*, vol. 24, no. 2, pp. 69–82, 2010.

[9] H. Fanakubo, “Shape memory alloys.” Bell and Bain Ltd., Glasgow, 1984.

[10] C. Darjan, “Shape memory alloys,” Univerza Ljubljani, 2007.

[11] K. Worden, W. A. Bullough, and J. (Jonathan) Haywood, *Smart technologies*. World Scientific, 2003.

[12] G.S Firstov, J. Humbeeck, and Y. Koval, “High-temperature shape memory alloys: Some recent developments,” *Mater. Sci. Eng. A*, vol. 378, no. 1–2, pp. 2–10, Jul. 2004.

[13] T. W. Duerig, J. Albrecht, and G. H. Gessinger, “A shape memory alloy for high-temperature applications,” *J. Met.*, vol. 34, no. 12, pp. 14–20, 1982.

[14] S. Padula Ii, G. Bigelow, R. Noebe, D. Gaydosh, and A. Garg, “Challenges and Progress in the Development of High-Temperature Shape Memory Alloys Based on NiTiX Compositions for High-Force Actuator Applications.” Cleveland, p. 9, 2006.

[15] J. Ma, I. Karaman, and R. D. Noebe, “High temperature shape memory alloys,” *Int. Mater. Rev.*, vol. 55, no. 5, pp. 257–315, Sep. 2010.

[16] Y Wu, X Lio, X Chen, X Hui, Y Zhang, and Z.P Lu, “Designing Bulk Metallic Glass Composites with Enhanced Formability and Plasticity,” *J. Mater. Sci. Technol.*, vol. 30, no. 6, pp. 566–575, Jun. 2014.

[17] M. Pohl, C. Heibing, and J. Frenzel, “Electrolytic processing of NiTi shape memory alloys,” *Mater. Sci. Eng. A*, vol. 378, no. 1–2, pp. 191–199, Jul. 2004.

[18] M. Mattson, *CNC programming : principles and applications*. Delmar, Cengage Learning, 2010.

[19] N. Sandberg, “On the Machinability of High Performance Tool Steels,” Uppsala Universitet, 2012.

[20] Jan Van Humbeeck, “Non-medical applications of shape memory alloys,” *Mater. Sci. Eng.*, pp. 134–148, 1999.

[21] Fei Gao, Hua Deng, and Yi Zhang, “Hybrid actuator combining shape memory alloy with DC motor for prosthetic fingers,” *Sensors actuators A Phys.*, vol. 223, pp. 40–48, 2015.

[22] O. M. Pearson and D. E. Lieberman, “The aging of Wolff’s law: Ontogeny and responses to mechanical loading in cortical bone,” *Am. J. Phys. Anthropol.*, vol. 125, no. S39, pp. 63–99, Jan. 2004.

[23] Ronny Pfeifer, Christian W. Muller, Christof Hurschler, Stefan Kaierle, Volker Wesling, and Heinz Haferkamp, “Adaptable orthopedic shape memory implants,” in *The First CIRP Conference on Biomanufacturing*, 2013, pp. 253–258.

[24] D. Wever, J. Elstrodt, A. Veldhuizen, and J. v Horn, “Scoliosis correction with shape-memory metal: results of an experimental study,” *Eur. Spine J.*, vol. 11, no. 2, pp. 100–106, Apr. 2002.

[25] V. Giurgiutiu, C. A. Rogers, and J. Zuidervaart, “Incrementally adjustable rotor-blade tracking tab using SMA composites,” in *AIAA/ASCE/AHS/ASC Structures, Structural Dynamics, and Materials Conference*, 1997, p. 11.

[26] D. M. Elzey, A. Y. N. Sofla, and H. N. G. Wadley, “A bio-inspired high-authority actuator for shape morphing structures,” in *Smart structures and materials*, 2003, vol. 5053, p. 92.

[27] J. P. Davim, *Machining : fundamentals and recent advances*. Springer, 2008.

[28] M. Naresh Kumar, K. S. Subbu, and V. P. Krishna, “Vibration Assisted Conventional and Advanced Machining: A Review,” *Procedia Eng.*, vol. 97, pp. 1577–1586, 2014.

[29] D. E. Brehl and T. A. Dow, “Review of vibration-assisted machining,” *Precis. Eng.*, vol. 32, pp. 153–172, 2007.

[30] He Sui, Xiangyu Zhang, Xinggang Jiang, and Ruibiao Wu, “Feasibility study of high-

speed ultrasonic vibration titanium alloy," *J. Mater. Process. Technol.*, vol. 247, pp. 111–120, 2017.

[31] Ashwin Polishetty, Manikandakumar Shumugavel, Raj Kumar Singh, and Guy Littlefair, "Review of Vibration Assisted Machining of Titanium and Nickel Alloys," in *International Colloqium on Materials*, 2014.

[32] V. Sharma and P. M. Pandey, "Recent advances in ultrasonic assisted turning: A step towards sustainability," *Cogent Eng.*, vol. 3, no. 1, p. 1222776, Aug. 2016.

[33] Riaz Muhammad, Mohammad Sajid Hussain, Agostino Maurotto, Carsten Siemers, Anish Roy, and Vadim V. Silbershcmidt, "Analysis of a free machining α+β titanium alloy using conventional and ultrasonically assisted turning," *J. Mater. Process. Technol.*, vol. 214, no. 4, pp. 906–915, Apr. 2014.

[34] Riaz Muhammad, Agostino Maurotto, Murat Demiral, Anish Roy, and Vadim V. Silberschmidt, "Thermally enhanced ultrasonically assisted machining of Ti alloy," *CIRP J. Manuf. Sci. Technol.*, vol. 7, no. 2, pp. 159–167, Jan. 2014.

[35] Sandip Patil, Shashikant Joshi, Asim Tewari, and Suhas S. Joshi, "Modelling and simulation of effect of ultrasonic vibrations on machining of Ti6Al4V," *Ultrasonics*, vol. 54, no. 2, pp. 694–705, Feb. 2014.

[36] A Maurotto, R. Muhammad, A. Roy, V.I. Babitsky, and V.V. Silershmidt, "Comparing Machinability of Ti-15-3-3-3 and Ni-625 Alloys in Uat," *Procedia CIRP*, vol. 1, pp. 330–335, Jan. 2012.

[37] Chandra Nath, M. Rahman, and S.S.K Andrew, "A study on ultrasonic vibration cutting of low alloy steel," *J. Mater. Process. Technol.*, vol. 192–193, pp. 159–165, Oct. 2007.

[38] V. K. Astashev and V. I. Babitsky, "Ultrasonic cutting as a nonlinear (vibro-impact) process," *Ultrasonics*, vol. 36, pp. 89–96, 1998.

[39] E. Brinksmeier, W. Preuss, and R. Glaebe, "Single Point Diamond turning of Steel," in *Proc. of the 1sr international euspen conference*, 1999, pp. 446–449.

[40] E. Brinksmeier and R. Gläbe, "Elliptical Vibration Cutting of Steel with Diamond Tools." Bremen, Germany, pp. 3–4, 1999.

[41] Gi Dae Kim and Byoung Gook Loh, "Characteristics of chip formation in micro V-grooving using elliptical vibration cutting," *J. Micromechanics Microengineering*, vol. 17, no. 8, p. 1458, Jun. 2007.

[42] E. Shamoto and T. Moriwaki, "Study on Elliptical Vibration Cutting," *CIRP Ann. - Manuf. Technol.*, vol. 43, no. 1, pp. 35–38, 1994.

[43] T. Moriwaki and E. Shamoto, "Ultrasonic Elliptical Vibration Cutting," *Ann. CIRP*, vol. 44, no. 1, pp. 31–34, 1995.

[44] Chunxiang Ma, E shamoto, T Moriwaki, Yonghong Zhang, and Lijang Wang, "Suppression of burrs in turning with ultrasonic elliptical vibration cutting," *Int. J.*

Mach. Tools Manuf., vol. 45, no. 11, pp. 1295–1300, Sep. 2005.

[45] X. Fan and M. H. Miller, “Force Modeling in Vibration Assisted Cutting.” .

[46] N. Negishi, *Elliptical Vibration Assisted Machining with Single Crystal Diamond Tools*. 2003.

[47] E. Shamoto, N. Suzuki, and R. Hino, “Simulation of Elliptical Vibration Cutting Process with Thin Shear Plane Model,” in *ASPE*, 2007, pp. 64–69.

[48] J. Zhang, T. Cui, C. Ge, Y. Sui, and H. Yang, “Review of micro/nano machining by utilizing elliptical vibration cutting,” *Int. J. Mach. Tools Manuf.*, vol. 106, pp. 109–126, Jul. 2016.

[49] Y. Yang, Y. Pan, and P. Guo, “Structural coloration of metallic surfaces with micro/nano-structures induced by elliptical vibration texturing,” *Appl. Surf. Sci.*, vol. 402, pp. 400–409, 2017.

[50] S. Sandfeld, T. Hochrainer, M. Zaiser, and P. Gumbsch, “Continuum modeling of dislocation plasticity: Theory, numerical implementation, and validation by discrete dislocation simulations,” *J. Mater. Res.*, vol. 26, no. 5, pp. 623–632, Mar. 2011.

[51] Nikolaos Nikitas, “Dislocation-based continuum models of crystal plasticity on the micron scale,” University of Edinburgh, 2008.

[52] R Christopher Weinberger and J. G. Tucker, *Multiscale Materials Modeling for Nanomechanics*, vol. 245. Cham: Springer International Publishing, 2016.

[53] Andreas Uppstu, “Electronic properties of graphene from tight-binding simulations,” Aalto University, 2014.

[54] E. R. Hernández, “Molecular Dynamics: from basic techniques to applications (A Molecular Dynamics Primer).” Barcelona, Spain, p. 28.

[55] B.-J. Lee, W.-S. Ko, H.-K. Kim, and E.-H. Kim, “The modified embedded-atom method interatomic potentials and recent progress in atomistic simulations,” *CALPHAD Comput. Coupling Phase Diagrams Thermochem.*, vol. 34, pp. 510–522, 2010.

[56] Murray S. Daw and M.I. Baskes, “Embedded-atom method: Derivation and application to impurities, surfaces and other defects in metals,” *Phys. Rev. B*, vol. 29, no. 12, pp. 6444–6452, 1983.

[57] M. I. Baskes, “Modified embedded-atom potentials for cubic materials and impurities,” *Phys. Rev. B*, vol. 46, no. 5, pp. 2727–2742, Aug. 1992.

[58] S. Ryu, C. R. Weinberger, M. I. Baskes, and W. Cai, “Improved modified embedded-atom method potentials for gold and silicon,” *Model. Simul. Mater. Sci. Eng*, vol. 17, pp. 1–14, 2009.

[59] B. J. Lee and M. J. Baskes, “Second nearest-neighbor modified embedded-atom

method potentials," *Phys. Rev. B*, vol. 62, pp. 8564–8567, 2000.

[60] B. J. Lee, M. J. Baskes, H. Kim, and Y. K. Cho, "Second nearest-neighbor modified embedded atom method potentials for BCC transition metals," *Phys. Rev. B*, vol. 64, 2001.

[61] Y.-M. Kim and B.-J. Lee, "A modified embedded-atom method interatomic potential for the Cu–Zr system," *J. Mater. Res.*, vol. 23, no. 4, pp. 1095–1104, Apr. 2008.

[62] G Ghosh, "First-principles calculations of structural energetics of Cu-TM (TM = Ti, Zr, Hf) intermetallics," *Acta Mater.*, vol. 55, no. 10, pp. 3347–3374, 2007.

[63] K. Wedel, "Simulations of Mechanical Properties of CuZr and CuMg Metallic Glasses," Technical University of Denmark, 208AD.

[64] Q. Cheng, H. A. Wu, Y. Wang, and X. X. Wang, "Pseudoelasticity of Cu–Zr nanowires via stress-induced martensitic phase transformations," *Appl. Phys. Lett. Addit. Inf. Appl. Phys. Lett. J. Homepage*, vol. 95, 2009.

[65] H. Kato and K. Sasaki, "Transformation-induced plasticity as the origin of serrated flow in an NiTi shape memory alloy," *Int. J. Plast.*, vol. 50, pp. 37–48, Nov. 2013.

[66] K.-I. Saitoh and W. K. Liu, "Molecular dynamics study of surface effect on martensitic cubic-to-tetragonal transformation in Ni–Al alloy," *Comput. Mater. Sci.*, vol. 46, pp. 531–544, 2009.

[67] V. Candido de Sousa and C. De Marqui Junior, "Effect of pseudoelastic hysteresis of shape memory alloy springs on the aeroelastic behavior of a typical airfoil section," *J. Intell. Mater. Syst. Struct.*, vol. 27, no. 1, pp. 117–133, Jan. 2016.

[68] Gian Song *et al.*, "Martensitic transformation in a B2-containing CuZr-based BMG composite revealed by in situ neutron diffraction," *J. Alloys Compd.*, vol. 723, pp. 714–721, 2017.

[69] F. J. Gil, J. A. Planell, and C. Libenson, "Differences in the pseudoelasticity behaviour of nickel-titanium orthodontic wires," *J. Mater. Sci.*, vol. 4, pp. 281–284, 1993.

[70] Jifeng Wang, "Dislocation slip and twinning stress in shape memory alloys - theory and experiments," University of Illinois at Urbana-Champaign, 2013.